https://doi.org/10.5194/egusphere-2026-3345
Preprint. Discussion started: 15 September 2026


# ThawCoupler-1D (v1.0): A physically-based one-dimensional coupled thermo-mechanical model for simulating thaw subsidence in heterogeneous permafrost

Guoan Yin[1], Zhanju Lin[1], Fujun Niu[2], Jing Luo[1], Huini Wang[3], Hongye Yan[4], Zeyong Gao[1], Xin Ju[1], Wenbin Yuan[1,5]

[1] State Key Laboratory of Cryospheric Science and Frozen Soil Engineering, Northwest Institute of Eco-Environment and Resources, Chinese Academy of Sciences, Lanzhou 730000, China
[2] Yangtze River Delta Urban Wetland Ecosystem National Field Scientific Observation and Research Station, Shanghai Normal University, Shanghai 200234, China
[3] Wuhan Institute of Technology, Wuhan 430074, China
[4] China Academy of Railway Sciences Corporation Limited. Beijing 100049, China
[5] University of Chinese Academy of Sciences, Beijing 100049, China

*Correspondence to*: Guoan Yin (yinguoan@lzb.ac.cn) and Zhanju Lin (zhanjulin@lzb.ac.cn)

**Abstract.** Permafrost thaw subsidence threatens infrastructure across Arctic and high-altitude regions and alters local hydrology. However, predicting the magnitude and rate of this deformation remains difficult due to the complex mechanical behavior of heterogeneous ground ice. Existing land surface models (LSMs) typically represent subsidence as a simplified geometric volume loss, omitting the transient dissipation of pore water pressure. Conversely, highly detailed geotechnical models are computationally expensive, making them impractical for multi-decadal, climate-scale simulations. To resolve these limitations, we developed ThawCoupler-1D (v1.0), a physically-based, computationally efficient finite-difference model designed to simulate thaw subsidence across highly variable ground-ice conditions. The model implements a threshold-based algorithm that switches between two settlement modes based on the initial void ratio: (1) large-strain thaw consolidation for porous soil matrices, governed by coupled heat transfer and pore water pressure dissipation; and (2) volumetric collapse for massive ice bodies (e.g., ice wedges), governed by phase-change kinetics and structural failure. The model utilizes a vectorized numerical scheme with an adaptive time-stepping algorithm constrained by the Courant-Friedrichs-Lewy (CFL) condition, allowing stable multi-decadal simulations at sub-daily and millimeter-level resolutions. We verified the model against analytical benchmarks and evaluated its performance using in situ borehole observations from the Beiluhe basin on the Qinghai-Tibet Plateau. The results show that ThawCoupler-1D reproduces the seasonal zero-curtain effect in thermal profiles and captures the non-linear settlement dynamics of both segregated and massive ground ice. Projections under CMIP6 scenarios indicate a critical thermal threshold, beyond which massive ice undergoes rapid volumetric collapse. This open-source code provides a tool for investigating thermo-mechanical feedbacks in degrading permafrost landscapes and improving sub-grid parameterizations in Earth System Models (ESMs).

https://doi.org/10.5194/egusphere-2026-3345
Preprint. Discussion started: 15 September 2026


## 1 Introduction

Permafrost, defined as ground remaining at or below 0 °C for at least two consecutive years (Dobinski, 2011), underlies vast regions of the Arctic, Subarctic, and the Qinghai-Tibet Plateau (Obu et al., 2019; Yin et al., 2021a). A key feature of these areas is the prevalence of excess ground ice (i.e., ice volumes exceeding the natural pore space of the soil matrix), which is particularly abundant in syngenetic permafrost formed in cold depositional environments (Gilbert et al., 2016; French, 2007). Climate-driven ground warming and subsequent permafrost degradation have been widely documented across high-latitude and high-altitude regions (Biskaborn et al., 2019; Smith et al., 2022). Thawing of the ice-rich terrain leads to phase-change volume loss, manifesting as surface subsidence and thermokarst development in flat landscapes (Kokelj and Jorgenson, 2013; Streletskiy et al., 2025). This process threatens infrastructure integrity(Hjort et al., 2022; Jin et al., 2024) ) and alters local hydrology and ecosystem functions (Walvoord and Kurylyk, 2016; Creel et al., 2024). The magnitude and rate of subsidence depend heavily on the cryostratigraphy. While the melting of pore and segregated ice leads to time-dependent soil consolidation, the degradation of massive ice bodies (e.g., ice wedges or thick lenses) triggers rapid structural collapse (Kokelj and Jorgenson, 2013). Resolving this mechanical heterogeneity is therefore necessary for reliable long-term projections of permafrost hazards (Nitzbon et al., 2020). However, direct, continuous, high-resolution measurements of subsidence are often logistically constrained and costly in remote environments (Gruber, 2020; O’Neill et al., 2023; Streletskiy et al., 2025). This observational gap limits regional-scale settlement quantification and highlights the need for physically-based numerical models to translate point-scale observations to larger spatial scales.

Although numerical models have advanced the understanding of permafrost thermal dynamics in a warming world (e.g., Clow, 2018; Langer et al., 2024; Zhao et al., 2025), simulating thaw subsidence remains difficult due to the non-linear coupling of heat transfer, phase-change kinetics, and large-strain soil deformation (Westermann et al., 2016). For regional assessments, studies have historically relied on the Stefan equation paired with empirical thaw-strain metrics (Nelson et al., 2001; Yin et al., 2023). While computationally inexpensive, these static methods neglect the time-dependent physics of soil consolidation and the thermal feedback associated with soil compaction. To evaluate subsidence under climate change scenarios, excess-ice parameterizations have been integrated into process-based land surface models (LSMs), such as the Community Land Model (CLM) (Lee et al., 2014; Lawrence et al., 2019), CryoGrid 3 (Westermann et al., 2016; 2023), and the Advanced Terrestrial Simulator (ATS) (Painter et al., 2016). These models simulate macro-scale energy balances and biogeochemical cycles but represent the mechanics of subsidence via a simplified "geometric volume removal" strategy. By assuming instantaneous water drainage and surface lowering upon thawing, these models bypass the transient consolidation of the soil skeleton. This simplification can lead to overestimates of early-stage settlement rates in fine-grained, low-permeability soils (e.g., silty clays) and omits the dynamic feedback between soil densification and bulk thermal conductivity. Conversely, geotechnical finite-element models (e.g., Dumais and Konrad, 2017; Yu et al., 2020) solve large-strain thaw consolidation equations with high mechanical rigor, but their high computational cost restricts them from multi-decadal, climate-scale applications. Furthermore, finite-element formulations often encounter numerical singularities, known

https://doi.org/10.5194/egusphere-2026-3345
Preprint. Discussion started: 15 September 2026


as the "vanishing element" problem, when simulating the complete depletion of massive ice bodies, leading to numerical divergence.

Predicting the long-term trajectory of permafrost under future warming scenarios (e.g., CMIP6) presents additional difficulties. Traditional thermal models often project a gradual, linear increase in thaw depth. However, ice-rich permafrost possesses substantial thermal inertia due to latent heat buffering. This buffering can mask ongoing subsurface degradation until a thermal threshold is breached, after which abrupt volumetric collapse occurs (Jorgenson et al., 2015; Painter et al., 2023). Capturing this non-linear, threshold-driven tipping point is critical for infrastructure risk assessment but remains simplified in existing climate-scale modeling frameworks.

To resolve these competing limitations, we developed ThawCoupler-1D, a physically-based numerical model designed for the computationally efficient simulation of heterogeneous permafrost thaw settlement. The model implements a dual-mechanism coupling scheme within a Lagrangian moving-mesh framework. Using a threshold-based criterion governed by the initial void ratio, ThawCoupler-1D dynamically switches between large-strain consolidation equations (for soil matrices) and volumetric collapse logic (for massive ice).

ThawCoupler-1D is implemented as a fully vectorized finite-difference scheme. This structure avoids nested loop iterations, enabling efficient calculations across the entire soil profile. Combined with an adaptive time-stepping algorithm constrained by both thermal and hydraulic diffusivities, the model maintains numerical stability while maximizing calculation speed, making it suitable for multi-decadal projections. The objectives of this paper are to:

(1) Detail the mathematical formulation and numerical implementation of ThawCoupler-1D;

(2) Verify the model against analytical solutions  to ensure numerical accuracy and mass-energy conservation;

(3) Evaluate the model's performance using borehole observations from the Beiluhe basin on the Qinghai-Tibet Plateau, demonstrating its capability to simulate ground temperatures, active-layer dynamics, and differential thaw settlement.

## 2 Model Description

The ThawCoupler-1D model couples transient heat transfer with an updated Lagrangian framework for soil consolidation. The model domain is discretized into vertical control volumes (layers) where thermal properties and layer thicknesses are dynamically updated at each numerical time step.

### 2.1 Thermal dynamics

The thermal regime of the soil column is governed by the one-dimensional Fourier heat conduction equation, modified to incorporate the latent heat of fusion during phase transitions. To resolve the non-linearity associated with phase change without explicitly tracking the moving boundary (the Stefan problem), we employ the apparent heat capacity (AHC) formulation (Bonacina et al., 1973):

https://doi.org/10.5194/egusphere-2026-3345
Preprint. Discussion started: 15 September 2026


$$C_{app}(T)\frac{\partial T}{\partial t}=\frac{\partial}{\partial z}\left(\lambda_{eff}\frac{\partial T}{\partial z}\right) \tag{1}$$

where $T$ is the temperature (°C). $t$ is time (s), and $z$ is the vertical spatial coordinate (m). $\lambda_{eff}$ is the effective thermal conductivity (W m$^{-1}$K$^{-1}$), and $C_{app}$ is the volumetric apparent heat capacity (J m$^{-3}$K$^{-1}$).

The apparent heat capacity incorporates the sensible heat of the soil matrix and the latent heat contribution:

$$C_{app}=C_{sensible}+L\cdot\frac{\partial f_L}{\partial T} \tag{2}$$

$$C_{sensible}=(1-n)C_s+n\left(f_L C_w+(1-f_L)C_i\right) \tag{3}$$

where $C_s$, $C_w$, $C_i$ are the volumetric heat capacities of solid soil grains, water, and ice, respectively. $n$ is the porosity. $L$ is the volumetric latent heat of fusion (J m$^{-3}$), which is scaled by the total water content of the respective layer.

The phase change of pore water in soils occurs across a temperature range rather than at a singular point due to capillary and adsorption forces. The model defines a phase change interval between a freezing point depression (typically −0.2 ℃) and the transient melting point $T_{liquid}$ (0 ℃). The liquid water fraction, $f_L$, is parameterized as a linear function within this range:

$$f_L(T)=\begin{cases}1 & T\geq T_{liquid}\ (0\ ℃)\\ \dfrac{T-T_{solid}}{T_{liquid}-T_{solid}} & T_{solid}<T<T_{liquid}\\ 0 & T\leq T_{solid}\ (-0.2\ ℃)\end{cases} \tag{4}$$

where $T_{liquid}$=0 ℃ and $T_{solid}$ = −0.2 ℃ for the standard parameterization. This formulation ensures a smooth release of latent heat and provides a numerical buffer that stabilizes the adaptive time-stepping algorithm.

The effective thermal conductivity $\lambda_{eff}$ is parameterized using the geometric mean method (Johansen, 1975):

$$\lambda_{eff}=\lambda_s^{(1-n)}\cdot\lambda_w^{n\cdot f_L}\cdot\lambda_i^{n\cdot(1-f_L)} \tag{5}$$

where $\lambda_s$ $\lambda_w$ $\lambda_i$ are the thermal conductivities of soil grains, water, and ice. Crucially, as the soil consolidates (see Section 2.2), the porosity $n$ decreases, leading to a dynamic update of $\lambda_{eff}$, thereby capturing the thermo-mechanical feedback.

### 2.2 Mechanical framework

Unlike conventional models that rely on semi-empirical thaw-strain correlations, ThawCoupler-1D implements a coupled mechanical framework based on the one-dimensional consolidation theory of Morgenstern and Nixon (1971). The deformation behavior is determined by the effective stress principle and the dissipation of excess pore water pressure.

A key distinction in ThawCoupler-1D is the separation of reversible seasonal deformation from irreversible permafrost degradation. In natural settings, the active layer undergoes cyclic frost heave in winter and subsequent thaw settlement in summer, resulting in a net-zero annual volume change under stable climate conditions (Gruber, 2020). Geotechnically, the active layer behaves as an overconsolidated material, whereas the underlying ice-rich permafrost is structurally supported by

https://doi.org/10.5194/egusphere-2026-3345
Preprint. Discussion started: 15 September 2026


ground ice (Figures 1a-b). To prevent cumulative numerical artifacts from seasonal freeze-thaw cycles without requiring a computationally intensive frost-heave module, the model employs a virgin thaw tracking algorithm. Excess pore water pressure generation and subsequent large-strain consolidation are only initiated when the thermal front penetrates beyond the historical maximum active-layer depth (i.e., thawing intact permafrost for the first time).

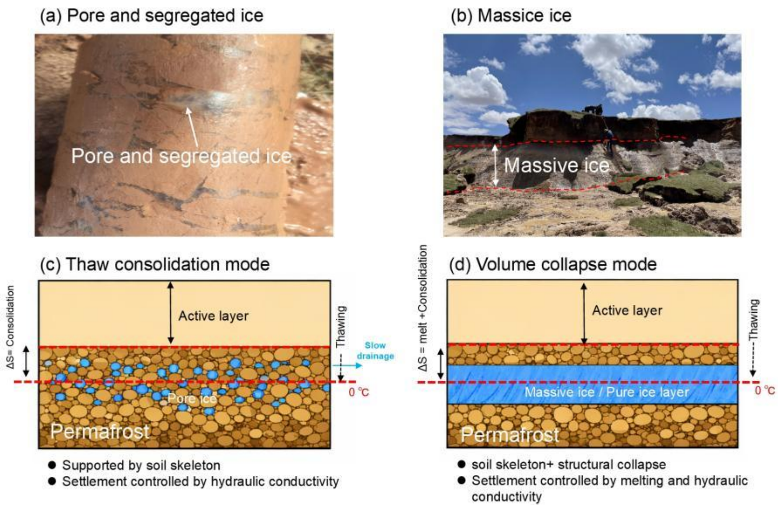


**Figure 1.** Schematic diagram of the physical model. (a) Core sample for pore and segregated ice in permafrost, (b) Photo of a retrogressive thaw slump showing massive ice layer in permafrost, (c) Thaw consolidation mode for ice-rich/poor permafrost, (d) volume collapse mode for massive ice permafrost.

To accommodate large strain (up to 50%) without solving the highly non-linear partial differential equation,.ThawCoupler-1D implements an updated Lagrangian approach where the coordinate system moves with the soil skeleton. The fundamental state variable is the void ratio ($e$), related to porosity by $n = \frac{e}{1+e}$.

For soil layers where ground ice is segregated within the soil matrix (defined by $e < e_{threshold}$), settlement is governed by the expulsion of excess pore water (Figure 1c). Upon thawing, the ice matrix melts, and the total overburden stress ($\sigma$) is transferred to the pore fluid, generating excess pore water pressure ($u$). The dissipation of this pressure is modeled as:

$$\frac{\partial u}{\partial t} = c_v \frac{\partial^2 u}{\partial z^2} \tag{6}$$

where $c_v$ is the coefficient of consolidation ($m^2\ s^{-1}$), defined as:

$$c_v = \frac{k}{m_v \gamma_w} \tag{7}$$

where $k$ is the hydraulic conductivity ($m\ s^{-1}$), $m_v$ is the coefficient of volume compressibility ($\mathrm{Pa}^{-1}$), and $\gamma_w$ is the unit weight of water. As pore pressure dissipates ($\Delta u$), the effective stress on the soil skeleton increases, resulting in volumetric strain ($\Delta\varepsilon$):

$$\Delta\varepsilon = m_v \cdot \Delta u \tag{8}$$

https://doi.org/10.5194/egusphere-2026-3345
Preprint. Discussion started: 15 September 2026


This strain results in the reduction of layer thickness ($\Delta z$) and the updating of the void ratio ($e$):

$$e_{new} = e_{old} - \Delta\varepsilon(1 + e_{old}) \tag{9}$$

For layers identified as massive ice (e.g., ice wedges or thick pure ice bands, where $e > e_{threshold} = 500$), the soil skeleton concept is invalid (Figure 1d). The threshold value of 500 corresponds to a porosity of approximately 99.8%, representing near-pure ice. This boundary is mathematically necessary. For massive ice, the coefficient of volume compressibility (Eq. 7) approaches zero ($m_v \rightarrow 0$), which causes an infinite $c_v$ ($\rightarrow \infty$). Consequently, the explicit stability criteria (Eq. 14) would dictate a vanishingly small time step ($\Delta t \rightarrow 0$), and induce numerical deadlock. Physically, these pure-ice control volumes bypass the consolidation solver. When the thermal module detects phase change in these elements, the model activates a volumetric collapse algorithm. Under free drainage assumptions, the settlement ($\Delta S$) is calculated as the thickness of the melted portion:

$$\Delta S_{collapse} = \Delta z_{melted} \tag{10}$$

To prevent non-physical pore pressure accumulation in free water, the excess pore pressure $u$ for these nodes is set to zero, acting as an internal drainage boundary for the underlying soil.

## 2.3 Numerical implementation

The coupled equations are solved using a finite difference method (FDM) implemented in MATLAB. To maintain physical fidelity while ensuring the computational efficiency required for multi-decadal simulations, ThawCoupler-1D employs a fully vectorized explicit scheme coupled with an adaptive time-stepping algorithm.

The soil domain is discretized into $N$ vertical control volumes. In our Lagrangian framework, the mass of solid particles within each control volume $i$ remains constant ($m_{s,i} = \rho_s(1-n_i)\Delta z_i$ = Constant), while the volume (and thus layer thickness $\Delta z_i$) varies due to consolidation. Unlike traditional iterative solvers that employ loop structures to update nodal states, ThawCoupler-1D utilizes matrix vectorization, leveraging modern CPU SIMD (Single Instruction, Multiple Data) instructions to minimize interpretation overhead in MATLAB. The explicit update for the thermal field is computed as::

$$\mathbf{T}^{t+\Delta t} = \mathbf{T}^{t} + \boldsymbol{\beta} \circ \left(\mathbf{T}_{i+1}^{t} - 2\mathbf{T}_{i}^{t} + \mathbf{T}_{i-1}^{t}\right) \tag{11}$$

where ∘ denotes the Hadamard (element-wise) product. and the stability coefficient vector $\boldsymbol{\beta}$ is derived dynamically at each step:

$$\boldsymbol{\beta} = \frac{\boldsymbol{\lambda}_{eff}}{\mathbf{C}_{app}} \cdot \frac{\Delta t}{(\Delta \mathbf{z})^2} \tag{12}$$

This vectorized approach handles highly heterogeneous stratigraphy where material properties vary abruptly between layers.

Explicit finite difference schemes are conditionally stable, governed by the Courant-Friedrichs-Lewy (CFL) condition. In a coupled thermo-mechanical problem, stability is constrained by the faster of the two physical processes: heat diffusion

https://doi.org/10.5194/egusphere-2026-3345
Preprint. Discussion started: 15 September 2026


or pore pressure dissipation. To ensure numerical stability while maximizing calculation speed, we implemented a Dual-Criterion Adaptive Time-Stepping algorithm. At the beginning of each iteration, the maximum permissible time step ($\Delta t$) is calculated as:

$$\Delta t_{thermal} = \min\left(\frac{0.5(\Delta \mathbf{z})^2}{\alpha_{th}}\right), \quad \alpha_{th} = \frac{\boldsymbol{\lambda}_{eff}}{\mathbf{C}_{app}} \tag{13}$$

$$\Delta t_{consol} = \min\left(\frac{0.5(\Delta \mathbf{z})^2}{c_v}\right), \quad c_v = \frac{\mathbf{k}}{\mathbf{m}_v \gamma_w} \tag{14}$$

$$\Delta t = \min(\Delta t_{thermal}, \Delta t_{consol}, \Delta t_{user\_limit}) \tag{15}$$

This logic allows the model to dynamically adjust its temporal resolution. During periods of rapid phase change (spring thaw) or high hydraulic gradients, $\Delta t$ automatically reduces to seconds or minutes to prevent numerical oscillation. During stable frozen periods (winter), $\Delta t$ expands to hours, accelerating the simulation.

The coupling between the thermal and mechanical modules is handled sequentially within each time step. The algorithm proceeds as follows (Figure 2) :

Step 1: Update parameters. Calculate dynamic properties ($\lambda_{eff}$, $k$, $C_{app}$) based on the current temperature $T$ and void ratio $e$.

Step 2: Time step calculation. Compute optimal $\Delta t$ using Eq. (15).

Step 3: Thermal solution. Solve the heat equation (Eq. 1) to obtain $T^{t+\Delta t}$.

Step 4: Phase change check. Identify nodes transitioning from frozen to thawed states. If pore ice ($e < e_{threshold}$), add effective overburden stress to the pore pressure vector $u$. If massive ice ($e \geq e_{threshold}$), trigger volumetric collapse logic, calculate settlement $\Delta S_{ice}$ immediately, and reset $u_i$=0.

Step 5: Mechanical solution. Solve the consolidation equation (Eq. 6) to update pore pressure $u^{t+\Delta t}$ and calculate consolidation settlement $\Delta S_{consol}$.

Step 6: Grid update (Lagrangian). Update layer thickness $\Delta z$ and void ratio $e$ based on total strain: $\Delta z^{t+\Delta t} = \Delta z^t - (\Delta S_{ice} + \Delta S_{consol})$.

This sequential coupling ensures that the thermal properties used in the next step reflect the densification of the soil, closing the thermo-mechanical feedback loop. All model paramater definitions and values can are listed in Table 1.

To verify the numerical stability and conservation of the sequential explicit coupling scheme, we monitored both the mass and energy balances of the system at each time step. First, mass conservation is strictly maintained by the Lagrangian grid formulation. The total volume of water expelled via consolidation matches the integrated strain across the thawed domain to machine precision ( $< 10^{-14}$ m), eliminating mass leakage. Second, energy conservation during phase change is ensured by integrating the apparent heat capacity ($C_{app}$) curve. The sequential coupling uses a conservative safety factor of 0.5 in the CFL criteria (Eq. 13-15). This ensures that the dynamic update of the grid coordinates ($\Delta z$) and bulk properties ($k_{eff}$,

https://doi.org/10.5194/egusphere-2026-3345
Preprint. Discussion started: 15 September 2026


$C_{app}$) does not introduce operator-splitting instabilities. Numerical testing across varied spatial resolutions ($\Delta z$ = 0.01 to 0.10m) confirmed that the solver converges monotonically without artificial energy drift.

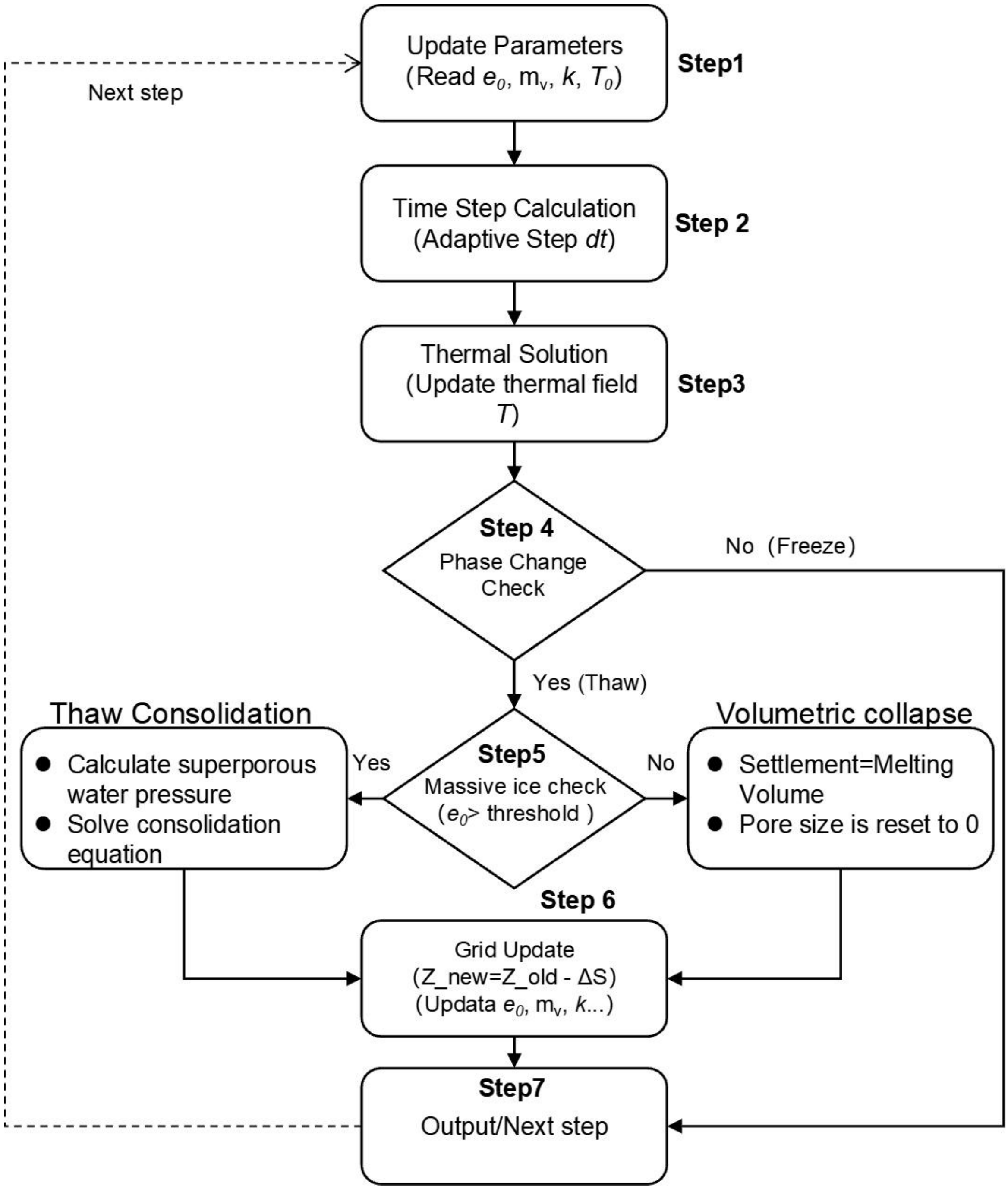


205 **Figure 2.** Workflow diagram of the ThawCoupler-1D model.

https://doi.org/10.5194/egusphere-2026-3345
Preprint. Discussion started: 15 September 2026


**Table 1.** List of physical constants and model parameters used in ThawCoupler-1D.

| | Symbol | Parameter Description | Value / Range | Unit | Source / Note |
|---|---|---|---|---|---|
| Physical Constants | $\rho_w$ | Density of water | 1000 | kg m$^{-3}$ | Standard |
| | $\rho_i$ | Density of ice | 917 | kg m$^{-3}$ | Standard |
| | $\gamma_w$ | Unit weight of water | 9810 | N m$^{-3}$ | $\approx \rho_w \cdot g$ |
| | $L_{ref}$ | Volumetric latent heat (pure water) | 3.34×10$^{8}$ | J m$^{-3}$ | Standard |
| | $G_s$ | Specific gravity of soil solids | 2.70 | - | Mineral soil |
| Thermal Properties | $C_s$ | Volumetric heat capacity (solids) | 2.0×10$^{6}$ | J m$^{-3}$ K$^{-1}$ | Langer et al. (2024) |
| | $C_w$ | Volumetric heat capacity (water) | 4.18×10$^{6}$ | J m$^{-3}$ K$^{-1}$ | Standard |
| | $C_i$ | Volumetric heat capacity (ice) | 2.09×10$^{6}$ | J m$^{-3}$ K$^{-1}$ | Standard |
| | $\lambda_s$ | Thermal conductivity (solids) | [3.0, 4.0] | W m$^{-1}$ K$^{-1}$ | Quartz-rich |
| | $\lambda_w$ | Thermal conductivity (water) | 0.57 | W m$^{-1}$ K$^{-1}$ | Standard |
| | $\lambda_i$ | Thermal conductivity (ice) | 2.2 | W m$^{-1}$ K$^{-1}$ | Standard |
| | $\Delta T_{mushy}$ | Phase change interval | 0.2 | K | [-0.2, 0]°C |
| | $n_f$ | Freezing n-factor | [0.6, 0.9] | - | Site-dependent |
| | $n_t$ | Thawing n-factor | [0.9, 1.2] | - | Site-dependent |
| Mechanical Properties | $m_v$ | Coeff. of volume compressibility | [1.0×10$^{-7}$, 8.0×10$^{-6}$] | Pa$^{-1}$ | Stratigraphy-dependent |
| | $e_0$ | Initial void ratio | [0.5, 3.0 (>500)] | - | Stratigraphy-dependent |
| | $n$ | Porosity | [0.30, 0.70] | - | $n = e_0 / (1+e_0)$ |
| | $k$ | Hydraulic conductivity | [1.0×10$^{-9}$, 1.0×10$^{-7}$] | m s$^{-1}$ | Stratigraphy-dependent |
| | $e_{threshold}$ | Threshold for massive ice | 500 | - | Numerical criterion |
| Numerical Settings | $\Delta z$ | Vertical grid resolution | 0.05 | m | Lagrangian (Initial) |
| | $\Delta t_{min}$ | Minimum time step | 1×10$^{-4}$ | day | Adaptive |
| | $\Delta t_{max}$ | Maximum time step | 0.5 | day | Adaptive |
| | $Z_{bot}$ | Lower boundary depth | 15.0 | m | Heat flux ≈ 0 |
| | $T_{bot}$ | Lower boundary temperature | [-1, -2.5] | °C | Dirichlet BC |

## 3. Model Verification

A rigorous hierarchical verification protocol was designed to evaluate the numerical accuracy and physical consistency of ThawCoupler-1D before applying it to complex field conditions. Validating coupled thermo-mechanical models is challenging, as standard analytical solutions typically assume static boundaries and decoupled physics. We therefore implemented a three-stage verification strategy to isolate, evaluate, and couple the individual numerical modules.

### 3.1 Thermal verification with the Neumann Problem

To verify the numerical accuracy of the heat transfer solver and the apparent heat capacity (AHC) formulation, the model was benchmarked against the exact Neumann analytical solution for a semi-infinite freezing/thawing medium (Kurylyk and Hayashi, 2016). To satisfy the mathematical assumptions of the analytical solution, the numerical model was decoupled from the mechanical module by setting the coefficient of volume compressibility to near zero ($m_v \approx 0$). The non-

https://doi.org/10.5194/egusphere-2026-3345
Preprint. Discussion started: 15 September 2026


linear thermal property updates (the Johansen method) were bypassed, and the thermal conductivities of all phases (soil, water, ice) were fixed to a constant value. A step-change temperature boundary condition ($T_{initial} < 0$ °C, $T_{surface} > 0$ °C) was applied. The numerical performance was evaluated by calculating the Root Mean Square Error (RMSE) and Mean Relative Error (MRE) between the simulated thaw depth and the exact theoretical trajectory, which dictates that thaw depth propagates proportionally to the square root of time ($X \propto \sqrt{t}$) (Text S1).

The simulated thaw depth exhibits close agreement with the Neumann analytical solution, yielding an RMSE of 0.0178 m and an MRE of 3.22% over the verification period (Figure 3a). This sub-centimeter accuracy demonstrates that the vectorized finite-difference scheme and the AHC formulation correctly conserve energy and track the moving phase boundary without numerical oscillation.

### 3.2 Mechanical Linearity Verification with Morgenstern-Nixon Theory

The mechanical module was verified against the classical Morgenstern-Nixon (1971) one-dimensional thaw consolidation theory. According to this theory, under a constant thermal boundary condition, the resulting thaw settlement ($S$) in a homogeneous, saturated soil column must evolve linearly with the square root of time ($S \propto \sqrt{t}$). In this test, compressible soil parameters were restored ($m_v = 5.0 \times 10^{-6}$ Pa$^{-1}$), and a constant surface warming was applied. The fidelity of the mechanical solver was evaluated by applying a linear regression to the simulated settlement versus $\sqrt{t}$ and calculating the coefficient of determination ($R^2$) (Text S1).

The simulated thaw subsidence demonstrates a linear relationship with the square root of time ($R^2 = 0.966$; Figure 3b), aligning with the Morgenstern-Nixon formulation. The minor non-linear lag observed during the initial steps reflects the transient buildup and subsequent dissipation of pore water pressure before reaching the quasi-steady state, capturing the physical process of hydrodynamic retardation.

### 3.3 Thermo-mechanical coupling feedback and algorithm sensitivity

The third stage evaluated the dynamic feedback between soil deformation and thermal propagation enabled by the Lagrangian moving-mesh framework. As ice-rich permafrost thaws and consolidates, the physical thinning of the soil layers and the reduction in porosity ($n$) alter the bulk thermal conductivity, thereby affecting the subsequent heat transfer rate.To demonstrate this feedback, we conducted a comparative experiment: (1) an uncoupled (static grid) simulation where soil deformation was disabled ($m_v \approx 0$), serving as a baseline thermal diffusion scenario, and (2) a coupled (dynamic grid) simulation utilizing a highly compressible soil parameter ($m_v = 2.0 \times 10^{-3}$ Pa$^{-1}$) to accentuate the consolidation process.

The coupled dynamic simulation exhibited a shallower apparent thaw depth (distance from the subsiding surface to the thaw front) compared to the uncoupled static simulation (Figure 3c). This difference is a geometric consequence of the Lagrangian mesh update. As the thawing soil layers consolidate, the vertical dimensions of the mesh elements shrink. This geometric compaction reduces the apparent active-layer thickness relative to the subsiding surface, even though the absolute

https://doi.org/10.5194/egusphere-2026-3345
Preprint. Discussion started: 15 September 2026


thermal propagation relative to a fixed datum is enhanced by the increased thermal conductivity of the densified soil matrix (Section 6.1).

To evaluate the robustness of the threshold-based dual-mechanism algorithm, we conducted synthetic sensitivity simulations representing three archetypal ground-ice structures: ice-poor, ice-rich, and massive-ice profiles. Driven by a uniform atmospheric warming trend, the model yielded distinctly divergent deformation trajectories. The responses ranged from progressive, linear consolidation (for pore ice) to abrupt, step-wise structural collapse (for massive ice). These controlled experiments confirm that the initial void ratio threshold criterion effectively transitions the numerical solver between continuum and discontinuum mechanics, allowing the model to resolve the non-linear mechanical heterogeneity of permafrost degradation (Text S2).

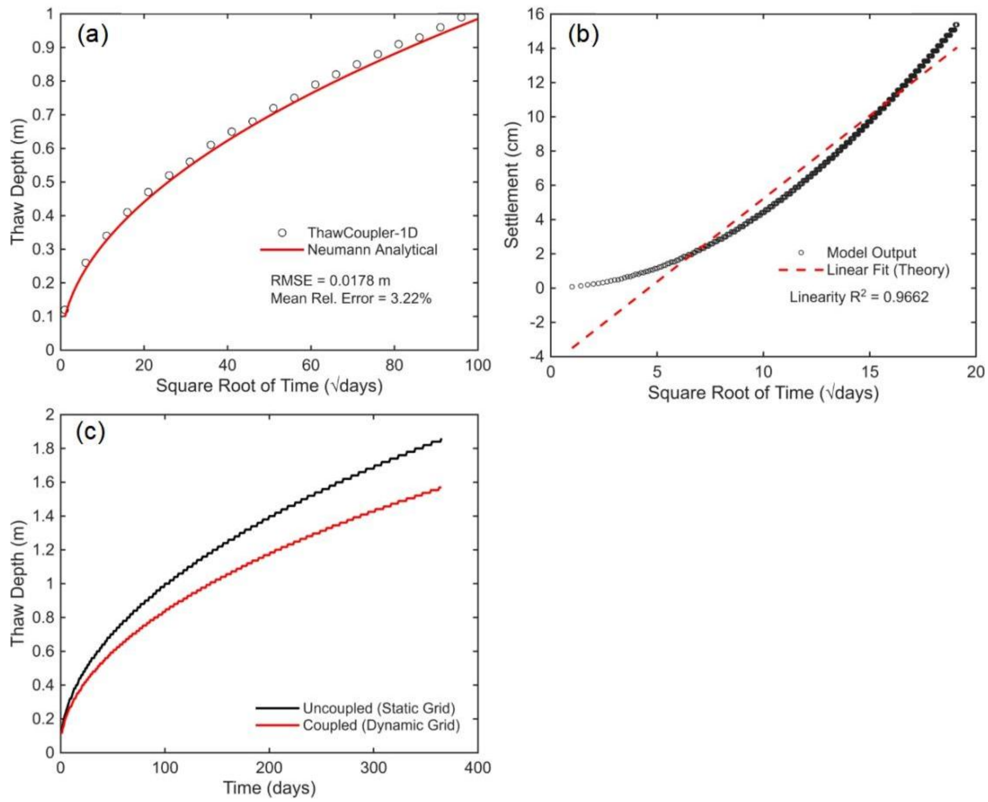


**Figure 3.** Model verification with analytical solutions.(a) Thermal verification with Neumann problem, (b) Mechanical verification with Morgenstern-Nixon theory, (c) Coupled feedback effect.

## 4. Model application to the Beiluhe basin

### 4.1 Study site and geocryological conditions

The Beiluhe basin (34.83 °N, 92.93 °E) is located in the hinterland of the QTP (Figure 4a).This area is underlain by continuous permafrost, characterized by an average elevation of 4,628 m a.s.l. and a semi-arid continental climate. The mean

https://doi.org/10.5194/egusphere-2026-3345
Preprint. Discussion started: 15 September 2026


annual air temperature (MAAT) ranges from−3.8 °C to −2.9 °C (Figure 4b), and the permafrost thickness varies between 20 and 80 m (Yin et al., 2017). Field monitoring by Lin et al. (2019) characterizes the permafrost here as "warm" (mean annual ground temperature between −1.5 °C and −0.5 °C), with ground-ice distribution exhibiting strong spatial heterogeneity largely controlled by local vegetation and lithology (Text S3; Lin et al., 2020).

To capture this spatial heterogeneity and evaluate the model's performance under different conditions, we defined three representative stratigraphic scenarios based on comprehensive borehole datasets from the basin (Table 2). These scenarios correspond to the dominant land cover types and ground-ice patterns found across the QTP (Figures 4c-e). The in situ datasets used to parameterize and validate these scenarios include vertical soil temperature and moisture profiles (at 0, 0.1, 2.5, and 5.0 m depths), air temperature (2 m above ground), soil texture, and measured ice content. While the continuous air temperature records span from 2006 to 2025, most subsurface measurements cover the 2016–2025 period. These field data serve as the basis for both generating the local meteorological forcing and evaluating model performance.

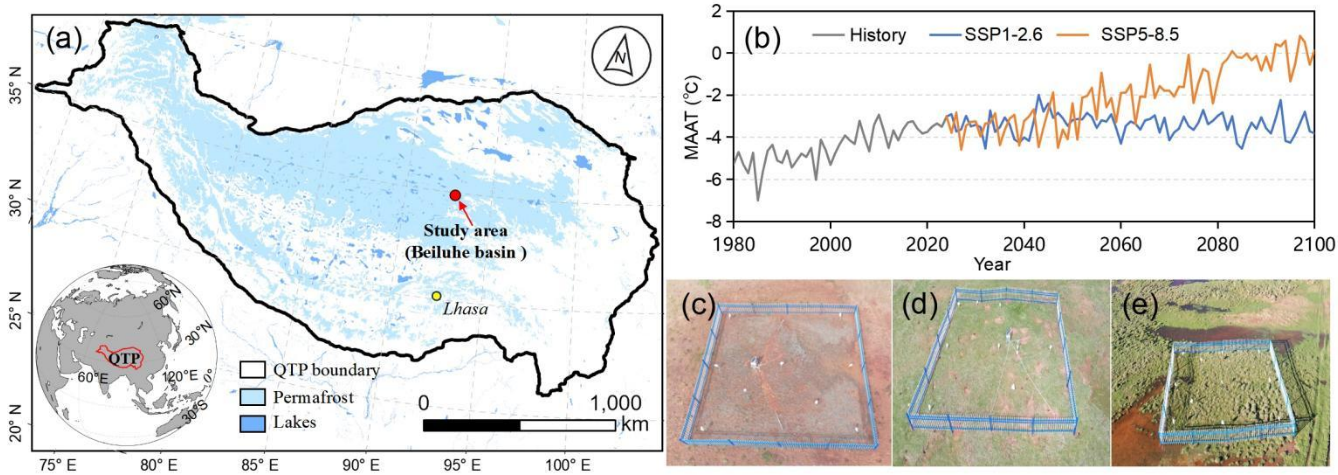


**Figure 4.** Study area and scenario configurations.(a) Location of the Beiluhe Basin on the Qinghai-Tibet Plateau. (b) Mean annual air temperature (MAAT) trends in the Beiluhe Basin from 1980 to 2100 under SSP1-2.6 and SSP5-8.5 scenarios. Representative site conditions for (c) Scenario A (Alpine desert, ice-poor), (d) Scenario B (Alpine meadow, excess-ice), and (e) Scenario C (Swamp meadow, massive-ice).

### 4.2 Meteorological forcing data

To drive the model over a multi-decadal timescale (1980 – 2100), we developed a continuous, hybrid daily meteorological forcing dataset. Because in situ observations are temporally limited, we applied a bias-correction approach to merge historical reanalysis data with future climate projections.

For the historical period (1980–2024), baseline daily air temperatures were extracted from the China Meteorological Forcing Dataset (CMFD) (He et al., 2020). To correct for systematic biases caused by coarse spatial resolution and elevation discrepancies, we established a linear transfer function using the overlapping period (2016 – 2024) between the nearest CMFD grid cell and the local automatic weather station (AWS) at Beiluhe.

For future projections (2025 – 2100), we used outputs from the AWI-CM-1-1-MR model under the SSP1-2.6 (low emissions) and SSP5-8.5 (high emissions) scenarios, as this model has shown superior performance in capturing historical temperature trends on the QTP (Chen et al., 2022b). To avoid artificial climate jumps at the historical-to-future boundary (2024/2025), we applied a trend-preserving monthly bias correction (Cannon et al., 2015). Specifically, we quantified the systematic bias of the global climate model by calculating the monthly climatological offset between its projections and the bias-corrected CMFD data during a decadal overlapping window. Subtracting this offset from the entire future time series ensures a seamless transition while strictly preserving the interannual variability and secular warming trends inherent in the SSP scenarios (Figure 4b).

Finally, the corrected daily air temperatures ($T_a$) were converted to upper-boundary ground surface temperatures ($T_s$) using site-specific freezing and thawing n-factors ($n_f$, $n_t$). These empirical factors account for the distinct surface energy balances governed by vegetation and snow cover at each site (Table 2; Lin et al., 2019).

**Table 2.** Stratigraphic and physical parameters for the three simulated scenarios in the Beiluhe basin. Parameter selection is based on field data from Lin et al. (2019, 2020).

| Depth (m) | Layer description | Void ratio ($e_0$) | Compressibility ($m_v$, Pa$^{-1}$) | Permeabilityk ($k$, m s $^{-1}$) | Latent heat ($L$, J m$^{-3}$) |
|---|---|---|---|---|---|
| Scenario A: Alpine desert and ice-poor, $n_t/n_f$ = 1.15 / 0.90 | | | | | |
| 0-10 | Homogeneous | 0.45 | 2.0 ×10 $^{-7}$ | 1.0 ×10 $^{-6}$ | 7.0×10$^{7}$ |
| Scenario B: Alpine meadow and ice-rich, $n_t/n_f$ = 0.85 / 0.65 | | | | | |
| 0-2.0 | Active Layer | 0.8 | 1.0 ×10 $^{-6}$ | 1.0 ×10 $^{-7}$ | 1.5 ×10$^{8}$ |
| **2.0-5.0** | Excess-Ice | 1.85 | 6.0 ×10 $^{-6}$ | 5.0 ×10 $^{-9}$ | 2.5 ×10$^{8}$ |
| 5.0-10 | Deep | 0.6 | 1.0 ×10 $^{-6}$ | 1.0 ×10 $^{-8}$ | 1.2 ×10$^{8}$ |
| Scenario C: Swamp meadow and massive-ice, $n_t/n_f$ = 0.95 / 0.7 | | | | | |
| 0-2.0 | Overburden | 1.2 | 2.0 ×10 $^{-6}$ | 5.0 ×10 $^{-8}$ | 1.8 ×10$^{8}$ |
| **2.0-5.0** | Massive Ice | **1000** | / | 0 | 3.3 ×10$^{8}$ |
| 5.0-10 | Deep | 0.8 | 1.0 ×10 $^{-6}$ | 1.0 ×10 $^{-9}$ | 1.4 ×10$^{8}$ |

### 4.3 Model setup and site-specific parameterization

To evaluate the model's capability across diverse cryolithological conditions, we parameterized the soil columns of the three scenarios using the physical properties listed in Table 2:

Scenario A characterizes high-altitude desert or steppe terrains (e.g., borehole BLH-10 in Lin et al., 2020, Figure 4c). These areas feature sparse vegetation cover (< 10%) and coarse-grained substrates (sands and gravels). Because the thin snow cover and lack of canopy shading strongly couple the ground surface to the atmosphere (Yin et al., 2026), we applied higher thawing n-factors ($n_t$ = 1.15) and freezing n-factors ($n_f$ = 0.90) to capture the intense solar absorption and rapid winter cooling (Lin et al., 2019). The soil column was parameterized as a homogeneous layer with a low initial void ratio ($e_0$ = 0.45,

https://doi.org/10.5194/egusphere-2026-3345
Preprint. Discussion started: 15 September 2026


corresponding to volumetric ice content VIC < 0.3) and low compressibility ($m_v$= 2.0×10$^{-7}$ Pa$^{-1}$), reflecting a rigid, grain-supported matrix.

Scenario B represents alpine meadow landscapes (e.g., borehole BLH-05; Figure 4d), dominated by dense vegetation and fine-grained silty soils. A defining geocryological feature here is the ice-rich transition layer located immediately beneath the active layer (Lin et al., 2020).To reflect the insulating effects of the summer canopy and winter snow trapping, the surface n-factors were reduced ($n_t$ = 0.85, $n_f$ = 0.65). The profile was vertically divided into three layers, with the critical transition layer (2.5–5.0 m depth) prescribed a medium high void ratio ($e_0$ = 1.85, VIC≈0.65) and high compressibility ($m_v$= 6.0×10$^{-6}$ Pa$^{-1}$) to represent the ice-rich silty clay reported by Lin et al. (2020). The hydraulic conductivity in this layer was constrained to a low value ($k$ = 5.0×10$^{-9}$ m s$^{-1}$) to appropriately simulate hydrodynamic retardation during thaw consolidation (Zhao et al., 2026; Gao and Coon, 2022).

Scenario C typifies localized areas underlain by massive ice bodies, frequently observed in swamp meadows or depressions (Figure 4e). We explicitly prescribed a pure ice layer between 2.5 m and 5.0 m depth by assigning an extreme void ratio ($e_0$ = 1000) that exceeds the numerical threshold. Upon thawing, this layer triggers the model's volumetric collapse algorithm, whereas the overlying and underlying soil layers continue to deform according to standard large-strain consolidation laws.

The simulation domain for all runs was set to a depth of 10.0 m with a vertical spatial resolution ($\Delta z$)of 0.05m. To establish equilibrium initial temperature profiles consistent with the local lithology, we utilized field-measured borehole data followed by a thermal spin-up phase that looped the 1980 climate forcing for 50 cycles. The upper boundary was driven by the hybrid daily surface temperature series (Section 4.2). The lower boundary condition was fixed at a constant temperature specific to each scenario, derived from regional field investigations (Yin et al., 2017). The transient simulations spanned from January 1, 1980, to December 31, 2100.

Beyond the baseline long-term projections, we utilized Scenario B as the primary benchmark for model evaluation. The simulated ground thermal regime was validated against in-situ borehole measurements using both quantitative statistical metrics and qualitative physical features (e.g., the zero-curtain effect).

## 5. Results

### 5.1 Comparison to field thermal measurements

The thermal performance of ThawCoupler-1D was evaluated by comparing simulated ground temperatures against in situ borehole monitoring datasets from the Beiluhe station (2016 – 2025). The model reproduces the transient thermal dynamics and seasonal freeze-thaw cycles of the active layer.

Figure 5 shows the continuous daily ground temperature comparison between the simulated and observed series at depths of 0.1 m, 2.5 m, and 5.0 m. At the shallow subsurface (0.1 m; Figure 5a), the simulated temperatures follow the observed series, capturing both the high-amplitude seasonal cycles and high-frequency synoptic fluctuations. This indicates

https://doi.org/10.5194/egusphere-2026-3345
Preprint. Discussion started: 15 September 2026


the validity of the applied n-factors (Table 2) in representing the surface energy balance under vegetation and snow cover. At a depth of 2.5 m (Figure 5b), which is situated within the highly compressible, ice-rich transition layer, the model reproduces the seasonal "zero-curtain" effect. During autumn freeze-back, the observed temperature remains near 0 °C due to latent heat release from the soil moisture. The model's ability to trace this isothermal plateau validates the apparent heat capacity (AHC) formulation, indicating that the latent heat budget of the transition layer is conserved. At 5.0 m depth (Figure 5c), both simulated and measured temperatures remain stable between −0.5 and −1.0 ℃, confirming the parameterization of the basal boundary condition and the frozen bulk thermal conductivity. The statistical consistency across these depths is summarized in the box plots (Figure 5d), showing matching medians, interquartile ranges, and temperature attenuation with depth, with minimal systematic bias.

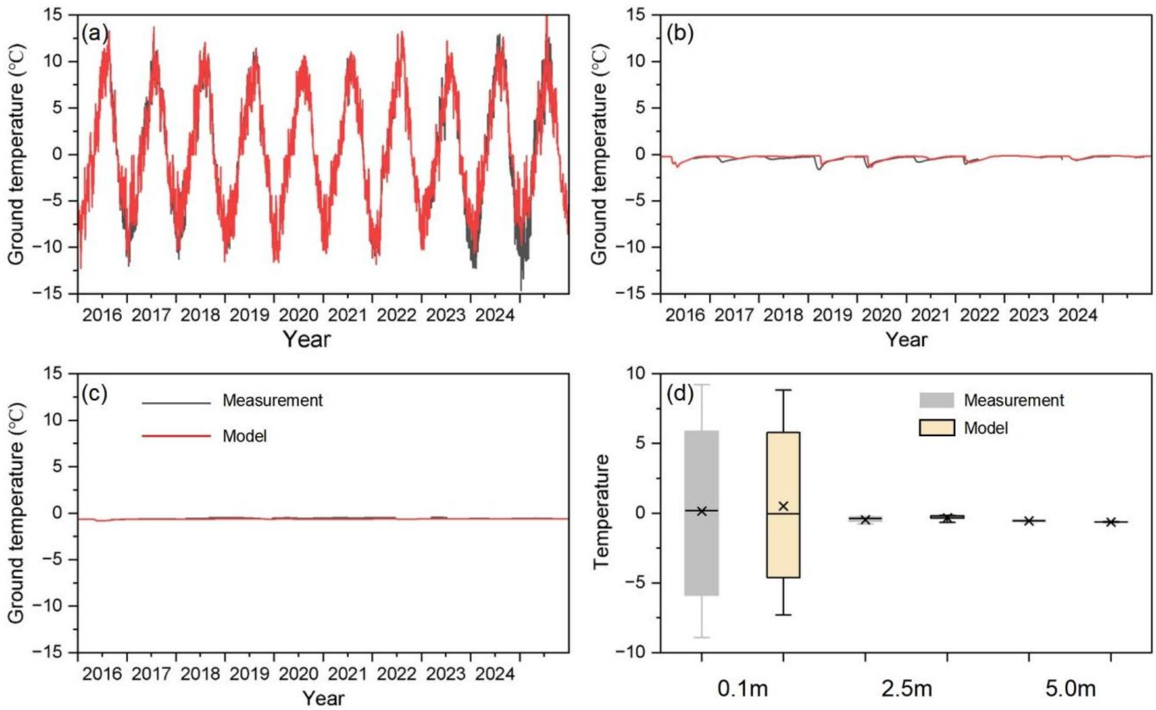


**Figure 5.** Modeled and measured ground temperatures for alpine meadow site at different depths. (a) 0.1m depth, (b) 2.5m depth, (c) 5.0 depth, (d) box plot of the comparison of the model with measurement for three depths.

The simulated interannual active-layer thickness (ALT) from 2016 to 2025 matches the observed interannual variability (Figure 6). The measured ALT, defined as the maximum annual depth of the 0 ℃ isotherm, fluctuates between 2.2 m and 2.6 m, showing a deepening trend from 2016 to 2020 followed by stabilization. The simulated ALT trajectory matches this trend, yielding a RMSE of 0.12 m.

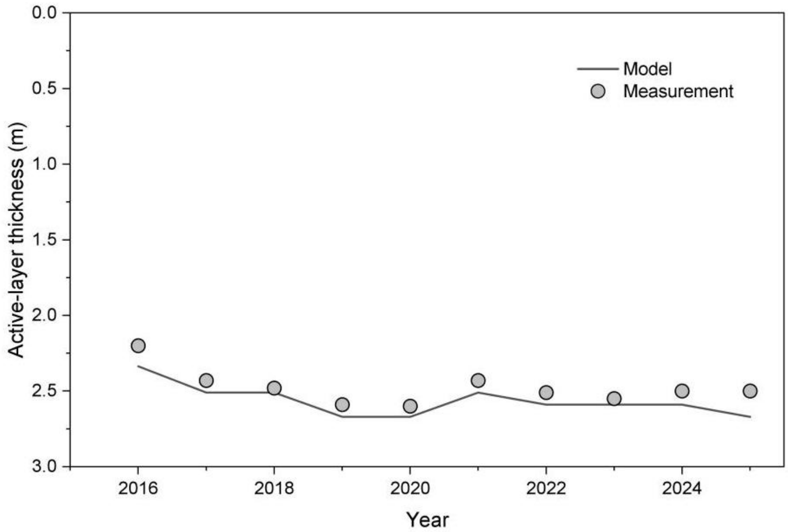


**Figure 6.** Modeled and measured annual max thaw depths (active-layer thickness) for alpine meadow site

### 5.2. Long-term thermal regime evolution

Figures 7 and 8 present the simulated spatio-temporal ground thermal regimes from 1980 to 2100 under the SSP1-2.6 and SSP5-8.5 scenarios. In these plots, the dynamic upper boundary directly reflects the continuous surface subsidence calculated by the Lagrangian mesh of ThawCoupler-1D.

Under the low-emission SSP1-2.6 scenario (Figure 7), the permafrost thermal regime eventually stabilizes. For all three cases, the active-layer base deepens until approximately 2050 and then maintains a relatively constant depth, with slight recovery observed toward the end of the century. In the massive-ice scenario (Figure 7c), the maximum thaw depth remains above the initial top of the massive ice table. Because the massive ice body is thermally preserved, the simulated ground surface elevation shows negligible change over the 120-year period. This suggests that limiting warming to the SSP1-2.6 levels may prevent the activation of massive ice collapse in the Beiluhe basin.

The SSP5-8.5 scenario (Figure 8) yields sustained, non-linear permafrost degradation. At the ice-poor alpine desert site (Scenario A, Figure 8a), the low latent heat content allows rapid downward heat propagation. By the 2070s, winter freezing no longer reaches the permafrost table, leading to the formation of a supra-permafrost talik (unfrozen zones > 0 °C persisting year-round). The development of this talik limits winter heat loss and further accelerates deep permafrost thaw, lowering the active-layer base beyond 6.0 m by 2100. An intermediate, yet highly dynamic, response is observed at the excess-ice alpine meadow site (Scenario B, Figure 8b). Compared to the ice-poor site, the downward propagation of the 0 °C isotherm is noticeably retarded due to the high latent heat demand of the ice-rich transition layer. However, continuous warming ultimately overcomes this thermal inertia. As the active-layer base progressively penetrates the ice-rich strata, it triggers large-strain thaw consolidation. Consequently, the ground surface experiences sustained, gradual subsidence, accompanied by a delayed but continuous deepening of the permafrost table and eventual talik formation.

https://doi.org/10.5194/egusphere-2026-3345
Preprint. Discussion started: 15 September 2026


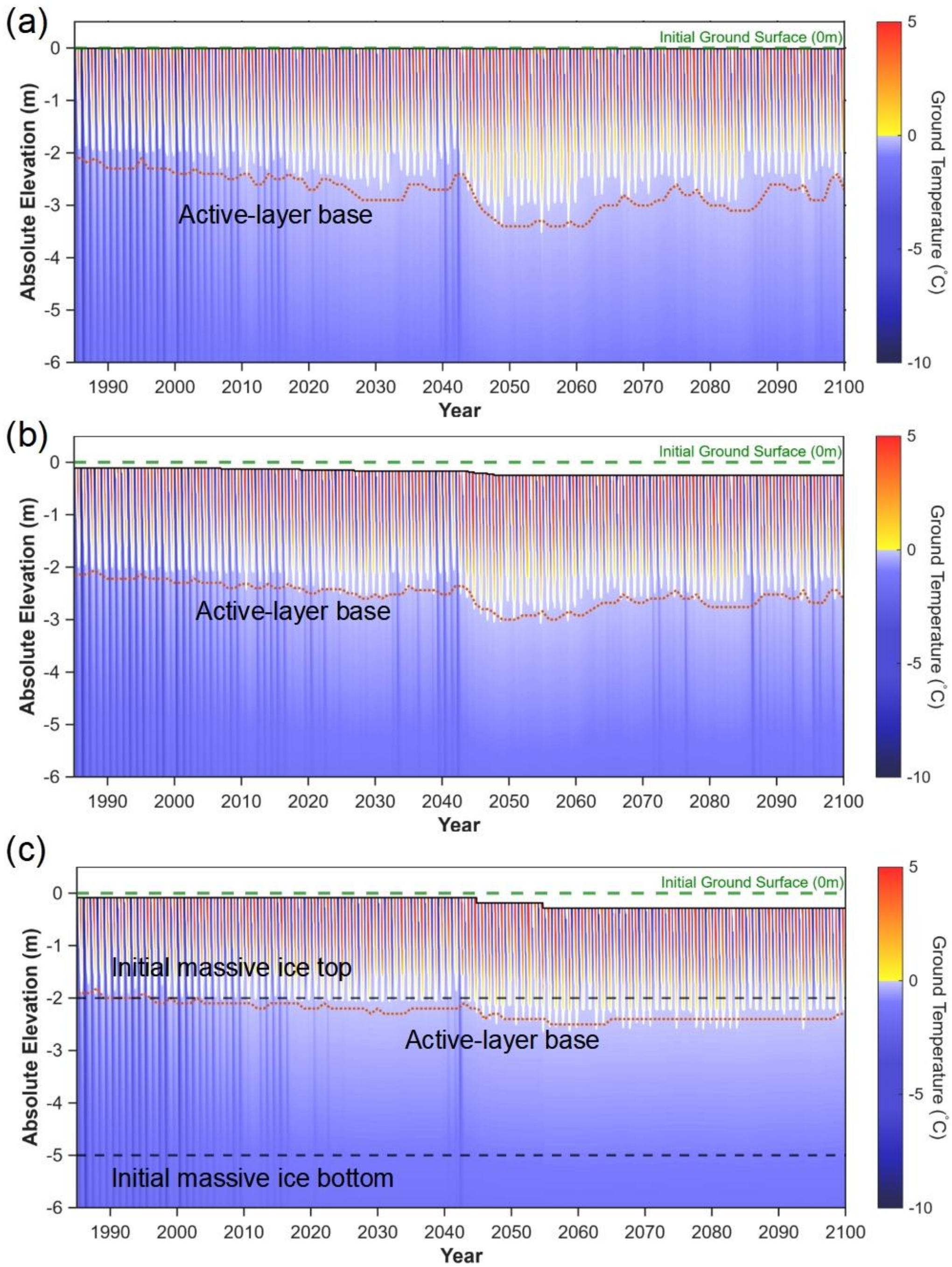


**Figure 7.** Modeled spatio-temporal evolution of the ground thermal regime from 1980 to 2100 under the SSP1-2.6 climate scenarios. (a) Scenario A (Alpine desert, ice-poor), (b) Scenario B (Alpine meadow, excess-ice), and (c) Scenario C (Swamp meadow, massive-ice). The dynamically updating upper boundary reflects the continuous surface subsidence calculated by the Lagrangian mesh, relative to the initial
385 ground surface.

https://doi.org/10.5194/egusphere-2026-3345
Preprint. Discussion started: 15 September 2026


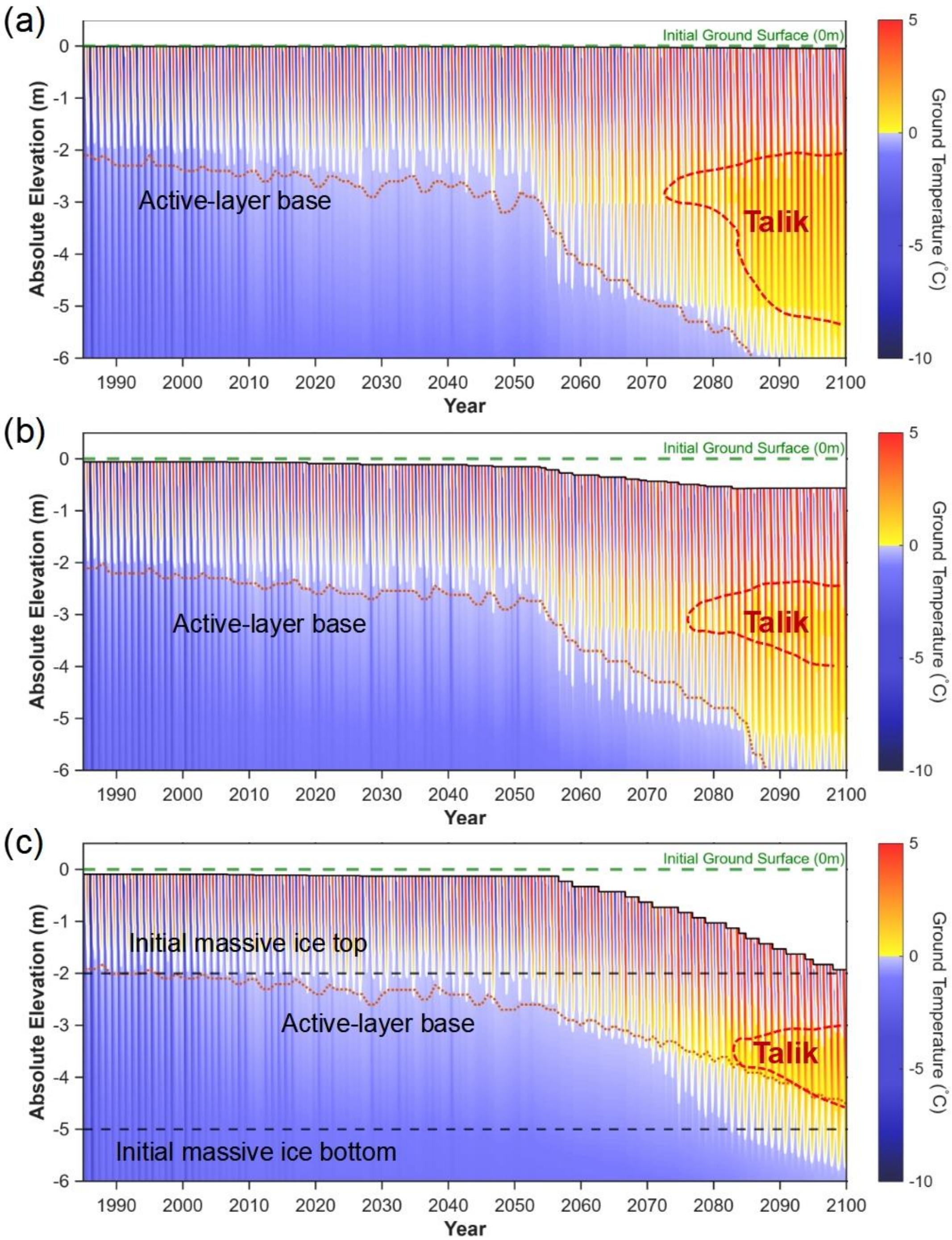


**Figure 8.** Modeled long-term ground temperature from 1980 to 2100 under the SSP5-8.5 climate scenario. (a) Scenario A (Alpine desert, ice-poor), (b) Scenario B (Alpine meadow, excess-ice), and (c) Scenario C (Swamp meadow, massive-ice). The formation of supra-permafrost taliks (unfrozen zones persisting year-round) is observable in the late 21st century.

The massive-ice scenario (Scenario C) exhibits a distinctly different thermal-mechanical response (Figure 8c). Between 1985 and 2050, the active-layer base deepens and intercepts the massive ice table (at 2.0 m depth relative to the initial surface). At this point, the downward propagation of the 0℃ isotherm largely stalls. This plateauing results from a strong latent heat buffering effect, where the phase change of massive ice consumes the available downward heat flux and temporarily restricts deeper thermal penetration. While the permafrost table depth appears stable during this period, the melting of massive ice simultaneously triggers substantial surface subsidence, evident from the steep drop in the upper domain boundary in Figure 8c. By the 2080s, the massive ice layer is completely depleted. The loss of this latent heat sink, combined with the densified soil overburden, subsequently permits rapid deep thaw and talik development.

These contrasting behaviors highlight the threshold-dependent nature of permafrost degradation in ice-rich terrains. The delayed yet abrupt onset of talik formation and massive ice collapse underscores why coupling latent heat kinetics with large-strain geometric deformation is indispensable for correctly projecting the timing and magnitude of thaw subsidence.

### 5.3 Thaw subsidence dynamics and cryostratigraphic controls

Building upon the thermal dynamics analyzed in Section 5.2, we evaluated the resulting mechanical deformation of the three distinct cryostratigraphies. Figure 9 illustrates the interannual evolution of the active-layer thickness (ALT) alongside the cumulative surface subsidence under both emission scenarios. The results highlight how subsurface ice distribution dictates the mechanical fate of the permafrost terrains.

Under the SSP1-2.6 scenario, the mechanical response is largely restricted by the stabilized thermal regime (Figures 9a, b). Because the maximum thaw penetration remains confined within the upper soil profile, the deeper excess and massive ice bodies are preserved. Consequently, cumulative subsidence for all three scenarios stabilizes by the mid-21st century. The ice-poor site (Scenario A) shows negligible deformation (<2 cm), while the ice-rich meadow (Scenario B) and massive-ice (Scenario C) sites accumulate approximately 25 to 30 cm of subsidence. This limited deformation corresponds primarily to the primary consolidation of the shallow overburden soil, indicating that mitigating warming to SSP1-2.6 levels is sufficient to avert deep structural failure in the Beiluhe basin.

Under the SSP5-8.5 scenario, the continuous downward propagation of the thermal front activates the deeper, ice-rich layers, leading to divergent subsidence pathways (Figures 9c, d). For the ice-poor alpine desert (Scenario A), despite the thaw front penetrating beyond 6.0 m by 2100, the cumulative subsidence remains nearly zero (<5 cm). This decoupled thermo-mechanical response reflects the behavior of a rigid, grain-supported soil matrix, where the phase change of low pore-ice content does not induce significant volume loss or structural compression. In contrast, the ice-rich alpine meadow (Scenario B) exhibits a progressive increase in subsidence, reaching approximately 60 cm by 2100. As the thaw front deepens beyond the historical active layer, the melting of the segregated ice within the transition layer transfers the overburden stress to the pore fluid. The subsequent dissipation of pore water pressure drives a continuous large-strain consolidation process, reflected in the gradual but sustained settlement curve.

https://doi.org/10.5194/egusphere-2026-3345
Preprint. Discussion started: 15 September 2026


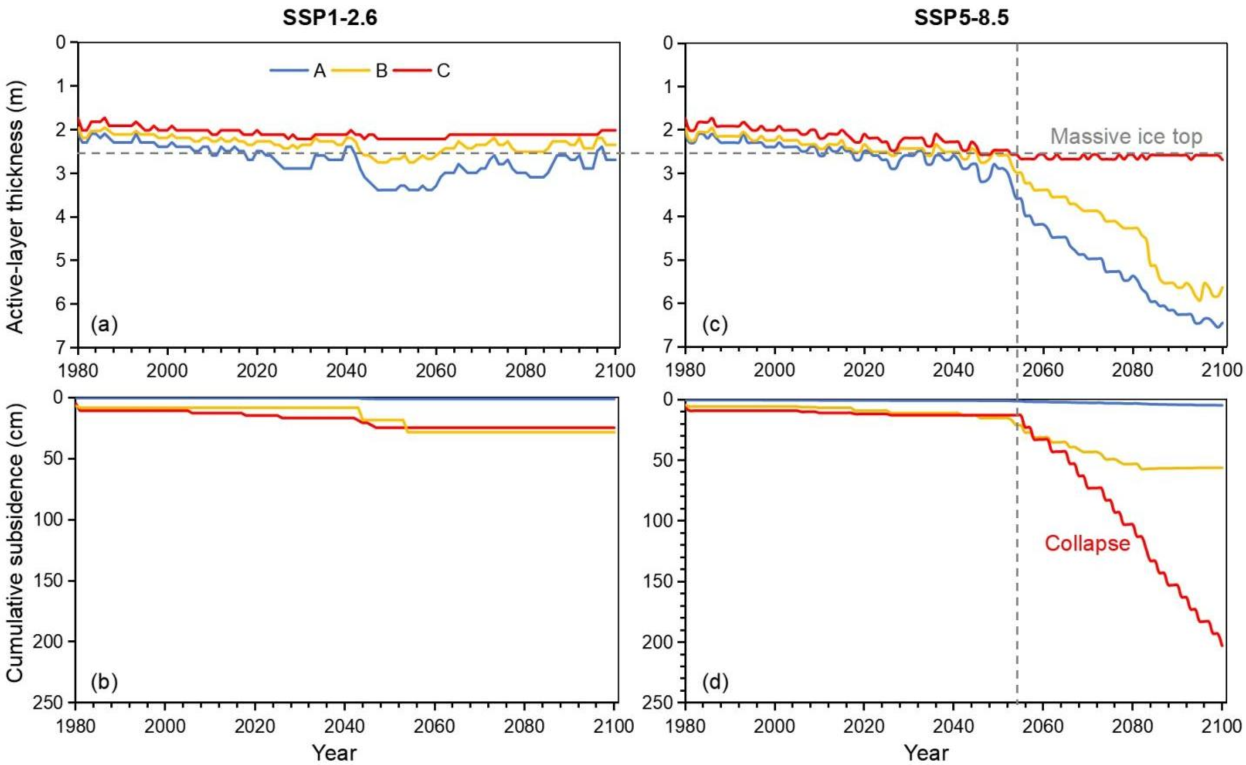


**Figure 9. Simulated interannual evolution of active-layer thickness and cumulative surface subsidence under the SSP1-2.6 (a, b) and SSP5-8.5 ( c, d) scenarios from 1980 to 2100.**

The most pronounced mechanical response occurs in the massive-ice scenario (Scenario C), where a thermo-mechanical shift is observed near the year 2055 (vertical dashed line in Figure 9c, d). Prior to 2055, the subsidence trajectory of Scenario C closely follows that of Scenario B, representing the consolidation of the soil overburden. Around 2055, the deepening active-layer base intercepts the top of the massive ice table (Figure 9c). At this exact juncture, the subsidence curve exhibits a sharp inflection (Figure 9d), transitioning into a rapid and persistent collapse phase. Notably, while the cumulative subsidence accelerates (exceeding 200 cm by 2100), the apparent active-layer thickness remains stable at approximately 2.6 m. This synchronous behavior represents the volumetric collapse mechanism implemented in ThawCoupler-1D: the latent heat of the massive ice absorbs the downward thermal flux, stalling further thermal penetration, while the melting ice translates into vertical surface lowering.

These results underscore that ground thermal indicators alone (such as ALT) are insufficient for assessing permafrost vulnerability. In regions underlain by massive ice, predicting the onset of thermokarst hazards requires a coupled framework capable of resolving the precise timing of ice-table intersection and the subsequent non-linear volume loss.

https://doi.org/10.5194/egusphere-2026-3345
Preprint. Discussion started: 15 September 2026


## 6. Discussion

The development and application of ThawCoupler-1D yield critical insights into the non-linear dynamics of permafrost degradation. By explicitly coupling heat transfer with consolidation and massive ice collapse, the model overcomes the inherent limitations of static empirical estimations and computationally prohibitive geotechnical simulations.

### 6.1 Densification and acceleration positive feedback mechanism

The Lagrangian framework of ThawCoupler-1D enables the quantification of a dynamic feedback between soil deformation and thermal propagation (Fig. 3c). Traditional Eulerian models, including most current Land Surface Models (LSMs), typically assume static soil porosities during thaw, thereby decoupling the mechanical state of the soil from its thermal evolution. Our results, however, indicate that this coupled formulation establishes a self-reinforcing densification-acceleration feedback loop.

As ice-rich permafrost thaws and excess pore water dissipates, the soil skeleton undergoes significant primary consolidation (Morgenstern and Nixon, 1971; Dumais and Konrad, 2018, Yu et al., 2020).This densification (i.e., a decrease in void ratio) intrinsically increases the volumetric fraction of highly conductive mineral solids relative to water or air (Côté and Konrad, 2005). Consequently, the bulk effective thermal conductivity of the thawed active layer increases. The consolidated soil acts as an evolving "thermal bridge", reducing the thermal resistance of the active layer and facilitating a more rapid downward sensible heat flux. Our decoupled sensitivity experiments demonstrate that neglecting this dynamic parameterization underestimates the absolute thaw depth by approximately 7 % under multi-decadal warming scenarios (Figure. 11). This indicates that permafrost degradation in compressible, ice-rich terrains (Schuur et al., 2015) can progress more rapidly than predicted by static thermal models.

Placing this mechanism within the broader context of permafrost degradation reveals an interplay between subsurface mechanics and surface hydrology. Recent modeling studies have primarily focused on surface-driven hydrological feedbacks. For example, Painter et al. (2023) demonstrated that thaw-induced subsidence can alter polygonal microtopography, increasing lateral runoff and drying the tundra surface. This surface drying acts as a negative feedback, where the desiccated peat and soil provide enhanced thermal insulation, limiting deeper permafrost thaw. Conversely, Nitzbon et al. (2020) highlighted a surface-driven positive feedback, where subsidence leads to localized water ponding. The high heat capacity and thermal conductivity of standing water accelerate the degradation of underlying ice wedges, triggering rapid thermokarst expansion. Our findings add a subsurface mechanical dimension to these feedbacks. The densification-acceleration feedback identified by ThawCoupler-1D acts as an internal accelerator. Even if surface drying occurs and provides top-down insulation (Painter et al., 2023), the simultaneous bottom-up compaction of the thawing soil matrix counters this effect by enhancing subsurface heat transfer. If, alternatively, the surface becomes waterlogged (Nitzbon et al., 2020), subsurface densification can act synergistically with surface ponding, potentially bringing the permafrost system toward its thermal tipping point sooner than projected by static-grid models. Ultimately, the long-term trajectory of ice-rich permafrost under

https://doi.org/10.5194/egusphere-2026-3345
Preprint. Discussion started: 15 September 2026


warming is governed by the competition between these surface hydro-ecological dynamics and subsurface thermo-mechanical densification.

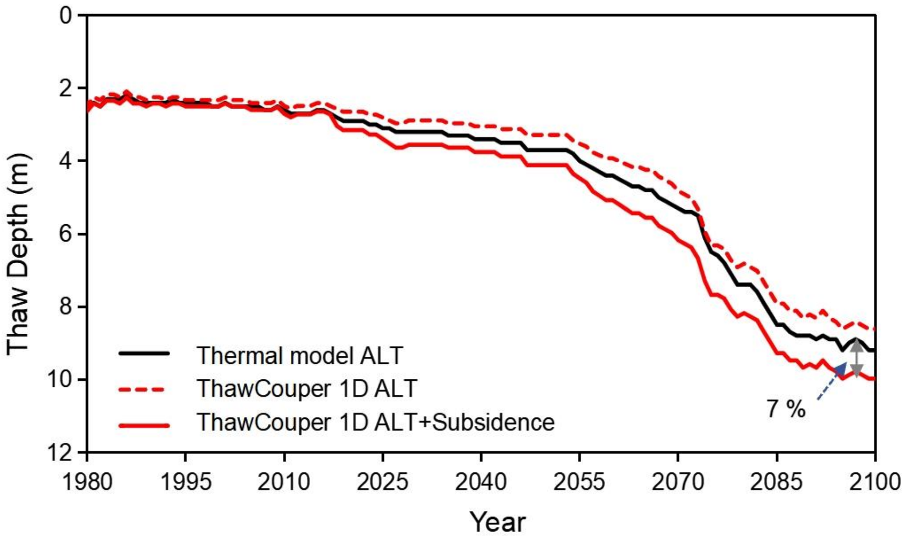


**Figure 10.** Comparison of long-term active-layer thickness (ALT) projections from 1980 to 2100 between the fully coupled ThawCoupler-1D model (dynamic feedbacks) and the uncoupled thermal model (static properties, mv≈0) under the SSP5-8.5 scenario for Scenario B. The black solid line represents the standard uncoupled thermal model. The red dashed line denotes the apparent ALT simulated by ThawCoupler-1D, measured relative to the dynamically subsiding ground surface. The red solid line represents the absolute thaw depth relative to the initial ground surface ($z$ = 0), calculated as the sum of the apparent ALT and the cumulative surface subsidence. The vertical double-headed arrow indicates that neglecting the coupled geo-mechanical feedback (the "densification-acceleration" effect) leads to a 7% underestimation of the absolute thaw depth by the end of the 21st century.

### 6.2 The latent heat shield and climate tipping points

Long-term projections under the CMIP6 scenarios (Section 5.3) demonstrate the role of cryostratigraphy in dictating the timing of geohazards. The simulations show that thaw subsidence in ice-rich terrain is non-linear and threshold-dependent.

Under the SSP5-8.5 scenario, the massive-ice system exhibits a period of stability for several decades. This thermal inertia is governed by the latent heat buffering effect: the energy required to phase-change the massive ice body restricts the downward sensible heat flux (Lee et al., 2014). During this induction period, the active-layer thickness (ALT) remains relatively stable, masking the underlying heat accumulation. Our sensitivity simulations demonstrate that the duration of this stability is sensitive to the thickness of the protective overburden. By systematically varying the initial depth of the massive ice table (from 1.0 m to 3.0 m), the model indicates that a thicker overburden delays the onset of structural failure (Text S4).

However, once the cumulative thermal forcing exhausts the protective capacity of the overburden, the thaw front intercepts the massive ice. This intersection triggers an abrupt shift, transitioning the system from continuous, slow consolidation into rapid, discontinuum volumetric collapse. This sudden onset of subsidence is consistent with abrupt thermokarst dynamics observed in the field (Kokelj and Jorgenson, 2013; Turetsky et al., 2020). Concurrently, this geometric collapse alters the local thermal boundary. As the massive ice ablates and the ground surface lowers, the

https://doi.org/10.5194/egusphere-2026-3345
Preprint. Discussion started: 15 September 2026


remaining soil column is often unable to completely refreeze during winter, leading to the rapid formation of a supra-permafrost talik (Figure 8; Connon et al., 2018; Farquharson et al., 2022). The emergence of a talik decouples the underlying permafrost from winter cooling, locking the system into a continuous degradation trajector (Farquharson et al. 2022).

These findings highlight a limitation in the current permafrost monitoring paradigm, which relies heavily on thermal indicators such as mean annual ground temperature (MAGT) or ALT (Smith et al., 2022). In ice-rich terrains, the latent heat shield effectively buffers thermal changes; ground temperatures may remain stable near 0 °C, and ALT may cease to deepen for decades, potentially misrepresenting the actual stability of the permafrost state (Farquharson et al., 2019). Yet, beneath this thermal equilibrium, the massive ice is actively decaying toward structural failure. Consequently, future geohazard assessments would benefit from transitioning from purely thermal metrics to coupled thermo-mechanical indicators to foresee impending climate tipping points.

### 6.3. Comparison with regional subsidence observations

While direct, point-scale validation of the mechanical module is currently limited by the lack of continuous, long-term geodetic measurements co-located with the studied boreholes, the simulated subsidence magnitudes and rates are consistent with regional observations across the QTP. This agreement provides a physical validation of ThawCoupler-1D.

For the excess-ice alpine meadow (Scenario B), the model simulates progressive thaw consolidation resulting in several decimeters of cumulative settlement, with an average rate of 2.0 mm yr$^{-1}$ over the initial decades of the simulation. This rate is consistent with the regional background subsidence rates (0.1-8 mm yr$^{-1}$) retrieved via persistent scatterer interferometry over the Beiluhe basin (Chen et al., 2022a). It also aligns with ground-based leveling measurements and independent modeling efforts along the Qinghai-Tibet Engineering Corridor (QTEC), which report annual subsidence rates ranging from 3.0 to 10.0 mm yr$^{-1}$ (Sun et al., 2022). This agreement suggests that the strain consolidation module reproduces the transient, water-pressure-limiting drainage process in thawing fine-grained soils. For the massive-ice scenario (Scenario C), ThawCoupler-1D projects an abrupt volumetric collapse exceeding 2.0 m over a decadal timescale once the protective latent heat shield of the overburden is breached. This surface lowering is supported by geomorphological field surveys in the Beiluhe basin. For instance, Niu et al. (2011) and Luo et al. (2022) documented that the melting of massive ground ice and subsequent thermokarst lake development cause ground surface collapse ranging from 0.4 m to over 3.0 m. Furthermore, long-term simulations demonstrate that the projected cumulative subsidence ultimately converges toward the static maximum subsidence potential derived from borehole ice contents (detailed in Text S3), verifying the mass conservation and physical validity of the mechanical module

The clear contrast between the progressive, decadal consolidation (Scenario B) and the rapid, multi-meter collapse (Scenario C) simulated by our model effectively captures the diverse modes of permafrost deformation observed in nature. This validation approach conforms to the up-to-date consensus proposed by Streletskiy et al. (2025), who argued that because establishing direct, continuous geodetic monitoring networks across vast and remote cold regions is logistically unfeasible, integrating physics-based, computationally efficient numerical models with localized cryostratigraphic and geodetic observations represents the most viable path forward to quantify and map permafrost subsidence at larger spatial scales.

### 6.4 Bridging geometric subtraction and hydrodynamic consolidation

A methodological contribution of ThawCoupler-1D is transitioning permafrost subsidence modeling from purely geometric approximations to dynamic thermo-mechanical coupling.

Recent advancements in 1D thermal models, such as FreeThawXice1D (Tubini and Gruber, 2025), have demonstrated solutions for maintaining energy conservation and adaptive mesh refinement during the phase change of pure excess ice. However, as noted by the developers, such thermal-centric models do not consider soil mechanics. In reality, the degradation of ice-rich permafrost—especially in the silty-clay transition layers widespread across the QTP (Lin et al., 2020), is governed by hydrodynamic impedance (Dumais and Konrad, 2018).

While the simplistic "geometric volume removal" strategy is effective for massive ice (Westermann et al., 2016), it assumes instantaneous drainage and compression. Our dual-mechanism approach bridges this gap. By solving the time-dependent dissipation of excess pore water pressure, our model captures the hydrodynamic lag in fine-grained, ice-rich soils (e.g., silty clay). This shows that actual physical settlement is retarded relative to the thermal phase-change front, providing a different timeline of infrastructure deformation compared to of instantaneous volume-subtraction methods. Furthermore, in conventional finite element methods (FEM), the complete melting of a massive ice element often leads to mesh entanglement or singularity matrices (Teng et al., 2022). By adopting a 1D finite-difference Lagrangian grid, our model handles this by smoothly reducing the layer thickness towards a numerical minimum while resetting hydraulic potentials. This allows the overburden to pass through the melted ice layer numerically, ensuring conservation of mass and energy without convergence failure.

### 6.5 Model implications and limitations

Current generation Earth System Models (ESMs), such as CLM5 (Lawrence et al., 2019), face challenges in capturing thaw subsidence: while they incorporate excess ice conceptually (Lee et al., 2014), the lack of geomechanical physics prevents them from representing the hydrodynamic lag and non-linear volumetric collapse observed in the field. ThawCoupler-1D provides an approach to address this limitation. By parameterizing complex THM (Thermo-Hydro-Mechanical) physics into a vectorized, adaptive-step 1D solver, ThawCoupler-1D can be a potential candidate for integration into global LSMs (such as future iterations of CLM) as a sub-grid mechanical parameterization scheme. Replacing the instantaneous volume-subtraction logic with our dual-mechanism consolidation algorithm would allow ESMs to dynamically compute effective ground subsidence. This, in turn, can provide dynamic boundaries for surface hydrological routing and permafrost carbon-climate feedback assessments (Turetsky et al., 2020).

However, certain simplifications warrant discussion for future improvements. As a 1D column model, ThawCoupler-1D assumes free vertical drainage and neglects lateral water routing. As shown by Painter et al. (2023) and Nitzbon et al. (2020),

https://doi.org/10.5194/egusphere-2026-3345
Preprint. Discussion started: 15 September 2026


lateral overland flow and localized ponding alter the surface energy balance, determining whether a degrading landscape becomes a well-drained high-centered polygon or a waterlogged thermokarst lake. Future versions of ThawCoupler-1D will aim to couple a surface routing module to address these lateral hydrological feedbacks (Aga et al., 2023). Additionally, integrating a cryosuction-driven frost heave module(Yu et al., 2019) is necessary to fully close the annual freeze-thaw deformation cycle.

## 7. Conclusion

In this study, we developed and validated ThawCoupler-1D, a physically-based numerical model designed to address the limitations of static geometric approximations in permafrost subsidence assessments. By coupling heat transfer with large-strain consolidation theory within a Lagrangian moving-mesh framework, the model provides a robust method to resolve the mechanical heterogeneity of ground ice. The primary conclusions are as follows:

(1) The threshold-based algorithm couples continuum consolidation and discontinuum collapse mechanics. This approach unifies the simulation of time-dependent, hydrodynamic consolidation in ice-rich soils with the rapid volumetric collapse of massive ice, resolving the numerical instabilities associated with the "vanishing element" problem in traditional finite-element methods. Verification against the analytical solution yields high numerical accuracy ($R^2$>0.96). Field application in the Beiluhe basin demonstrates that the model reproduces seasonal ground thermal dynamics, including the zero-curtain effect, and estimates realistic subsidence magnitudes.

(2) The dynamic updating of physical properties within the Lagrangian framework captures a subsurface positive feedback loop. As ice-rich soil thaws and consolidates, soil compaction increases the bulk thermal conductivity, acting as a thermal bridge that accelerates downward heat flux. This indicates that static-grid models can systematically underestimate long-term permafrost thaw rates.

(3) Projections under future warming scenarios (e.g., CMIP6 SSP5-8.5) show that massive ice bodies act as a temporary latent heat shield, stalling active-layer deepening for decades. However, once this thermal buffer is depleted, the active-layer base breaches the massive ice table, triggering an abrupt transition from gradual consolidation to rapid volumetric collapse. This demonstrates the insufficiency of relying solely on thermal metrics like active-layer thickness for geohazard monitoring.

(4) The vectorized finite-difference scheme and dual-criterion adaptive time-stepping algorithm ensure numerical stability while maintaining computational efficiency, allowing multi-decadal simulations at sub-daily resolutions within seconds on standard personal computers. This efficiency makes ThawCoupler-1D a viable candidate for integration into global Earth System Models as a sub-grid mechanical parameterization scheme.

ThawCoupler-1D provides an open-source tool for the cryosphere community to investigate the long-term evolution of permafrost landscapes. Future developments will focus on extending the framework to two dimensions to address lateral hydrological routing and integrating a cryosuction-driven frost heave module, which is necessary to simulate the complete annual freeze-thaw deformation cycle.

## Code and data availability

The source code of ThawCoupler-1D (v1.0) is archived on Zenodo at https://doi.org/10.5281/zenodo.20622154 (Yin, 2026). The repository includes the source scripts, the compilation of the Beiluhe case study parameters. The climate forcing data are available from the National Tibetan Plateau Data Center (http://data.tpdc.ac.cn). The borehole temperature data and soil physical property datasets from the Beiluhe basin used for model validation are available upon request from the corresponding author.

## Author contributions

GY developed the model code, designed the experiments, and wrote the original draft of the manuscript. ZL and FN provided the field data and overall project supervision. JL, HW, HY, ZG, XJ, and WY contributed to the data processing, analysis, and visualization. All authors participated in the critical review and editing of the final manuscript.

## Competing interests

The authors declare that they have no conflict of interest.

## Acknowledgements

We thank the staff at the Beiluhe Observation Station for their assistance in field data collection. During the preparation of this manuscript, the authors used AI-based tools for spelling, grammar editing to improve the readability of the English text. Computational algorithms and plotting scripts were conceived by the authors and verified with assistance from automated coding tools. The authors assume full responsibility for the scientific accuracy, originality, and integrity of the final manuscript contents.

## Financial support

This research was funded by National Natural Science Foundation of China ( U2468222; 42372334), Xizang Province's Major Science and Technology Project (XZ202601ZD0014), and Gansu Province's Major Science and Technology Project (25ZDFA013).

## References

Aga, J., Boike, J., Langer, M., Ingeman-Nielsen, T., and Westermann, S.: Simulating ice segregation and thaw consolidation in permafrost environments with the CryoGrid community model, The Cryosphere, 17, 4179–4206, 10.5194/tc-17-

https://doi.org/10.5194/egusphere-2026-3345
Preprint. Discussion started: 15 September 2026


4179-2023, 2023.

Biskaborn, B. K., Smith, S. L., Noetzli, J., Matthes, H., Vieira, G., Streletskiy, D. A., Schoeneich, P., Romanovsky, V. E., Lewkowicz, A. G., and Abramov, A.: Permafrost is warming at a global scale, Nature communications, 10, 264, 2019.

Bonacina, C., Comini, G., Fasano, A., and Primicerio, M.: Numerical solution of phase-change problems, International Journal of Heat and Mass Transfer, 16, 1825–1832, https://doi.org/10.1016/0017-9310(73)90202-0, 1973.

Cannon, A. J., Sobie, S. R., and Murdock, T. Q.: Bias Correction of GCM Precipitation by Quantile Mapping: How Well Do Methods Preserve Changes in Quantiles and Extremes?, Journal of Climate, 28, 6938–6959, https://doi.org/10.1175/JCLI-D-14-00754.1, 2015.

Chen, J., Wu, T., Zou, D., Liu, L., Wu, X., Gong, W., Zhu, X., Li, R., Hao, J., Hu, G., Pang, Q., Zhang, J., and Yang, S.: Magnitudes and patterns of large-scale permafrost ground deformation revealed by Sentinel-1 InSAR on the central Qinghai-Tibet Plateau, Remote Sensing of Environment, 268, 112778, https://doi.org/10.1016/j.rse.2021.112778, 2022a.

Chen, R., Li, H., Wang, X., Gou, X., Yang, M., and Wan, G.: Surface air temperature changes over the Tibetan Plateau: Historical evaluation and future projection based on CMIP6 models, Geoscience Frontiers, 13, 101452, https://doi.org/10.1016/j.gsf.2022.101452, 2022b.

Clow, G. D.: CVPM 1.1: a flexible heat-transfer modeling system for permafrost, Geosci. Model Dev., 11, 4889–4908, 10.5194/gmd-11-4889-2018, 2018.

Connon, R., Devoie, É., Hayashi, M., Veness, T., and Quinton, W.: The Influence of Shallow Taliks on Permafrost Thaw and Active Layer Dynamics in Subarctic Canada, Journal of Geophysical Research: Earth Surface, 123, 281–297, https://doi.org/10.1002/2017JF004469, 2018.

Côté, J. and Konrad, J.-M.: A generalized thermal conductivity model for soils and construction materials, Canadian Geotechnical Journal, 42, 443–458, 10.1139/t04-106, 2005.

Creel, R., Guimond, J., Jones, B. M., Nielsen, D. M., Bristol, E., Tweedie, C. E., and Overduin, P. P.: Permafrost thaw subsidence, sea-level rise, and erosion are transforming Alaska's Arctic coastal zone, Proceedings of the National Academy of Sciences, 121, e2409411121, doi:10.1073/pnas.2409411121, 2024.

Dobinski, W.: Permafrost, Earth-Science Reviews, 108, 158–169, https://doi.org/10.1016/j.earscirev.2011.06.007, 2011.

Dumais, S. and Konrad, J.-M.: One-dimensional large-strain thaw consolidation using nonlinear effective stress – void ratio – hydraulic conductivity relationships, Canadian Geotechnical Journal, 55, 414–426, 10.1139/cgj-2017-0221, 2017.

Farquharson, L. M., Romanovsky, V. E., Kholodov, A., and Nicolsky, D.: Sub-aerial talik formation observed across the discontinuous permafrost zone of Alaska, Nature Geoscience, 15, 475–481, 10.1038/s41561-022-00952-z, 2022.

Farquharson, L. M., Romanovsky, V. E., Cable, W. L., Walker, D. A., Kokelj, S. V., and Nicolsky, D.: Climate Change Drives Widespread and Rapid Thermokarst Development in Very Cold Permafrost in the Canadian High Arctic, Geophysical Research Letters, 46, 6681–6689, https://doi.org/10.1029/2019GL082187, 2019.

French, H. M.: Permafrost, in: The Periglacial Environment, 83–115, https://doi.org/10.1002/9781118684931.ch5, 2007.

Gao, B. and Coon, E. T.: Evaluating simplifications of subsurface process representations for field-scale permafrost hydrology models, The Cryosphere, 16, 4141–4162, 10.5194/tc-16-4141-2022, 2022.

Gilbert, G. L., Kanevskiy, M., and Murton, J. B.: Recent Advances (2008–2015) in the Study of Ground Ice and Cryostratigraphy, Permafrost and Periglacial Processes, 27, 377–389, https://doi.org/10.1002/ppp.1912, 2016.

Gruber, S.: Ground subsidence and heave over permafrost: hourly time series reveal interannual, seasonal and shorter-term movement caused by freezing, thawing and water movement, The Cryosphere, 14, 1437–1447, 10.5194/tc-14-1437-2020, 2020.

He, J., Yang, K., Tang, W., Lu, H., Qin, J., Chen, Y., and Li, X.: The first high-resolution meteorological forcing dataset for land process studies over China, Scientific Data, 7, 25, 10.1038/s41597-020-0369-y, 2020.

Hjort, J., Streletskiy, D., Doré, G., Wu, Q., Bjella, K., and Luoto, M.: Impacts of permafrost degradation on infrastructure, Nature Reviews Earth & Environment, 3, 24–38, 2022.

Jin, H., Peng, X., Frauenfeld, O. W., Huang, Y., Guo, L., Luo, J., Yin, G., Zhao, G., and Mu, C.: The infrastructure cost of permafrost degradation for the Northern Hemisphere, Global Environmental Change, 84, 102791, 2024.

Johansen, O. (1975). Thermal Conductivity of Soils. Ph.D. thesis, Norwegian University of Science and Technology (NTH), Trondheim, Norway. 231 pages. Later translated into English as CRREL Draft Translation 637 (1977), U.S. Army Cold Regions Research and Engineering Laboratory, Hanover, New Hampshire.

Jorgenson, M. T., Kanevskiy, M., Shur, Y., Moskalenko, N., Brown, D. R. N., Wickland, K., Striegl, R., and Koch, J.: Role

https://doi.org/10.5194/egusphere-2026-3345
Preprint. Discussion started: 15 September 2026


of ground ice dynamics and ecological feedbacks in recent ice wedge degradation and stabilization, Journal of Geophysical Research: Earth Surface, 120, 2280–2297, https://doi.org/10.1002/2015JF003602, 2015.

Kokelj, S. V. and Jorgenson, M. T.: Advances in Thermokarst Research, Permafrost and Periglacial Processes, 24, 108–119, https://doi.org/10.1002/ppp.1779, 2013.

Kurylyk, B. L. and Hayashi, M.: Improved Stefan Equation Correction Factors to Accommodate Sensible Heat Storage during Soil Freezing or Thawing, Permafrost and Periglacial Processes, 27, 189–203, https://doi.org/10.1002/ppp.1865, 2016.

Langer, M., Nitzbon, J., Groenke, B., Assmann, L. M., Schneider von Deimling, T., Stuenzi, S. M., and Westermann, S.: The evolution of Arctic permafrost over the last 3 centuries from ensemble simulations with the CryoGridLite permafrost model, The Cryosphere, 18, 363–385, 10.5194/tc-18-363-2024, 2024.

Lawrence, D. M., Fisher, R. A., Koven, C. D., Oleson, K. W., Swenson, S. C., Bonan, G., Collier, N., Ghimire, B., van Kampenhout, L., Kennedy, D., Kluzek, E., Lawrence, P. J., Li, F., Li, H., Lombardozzi, D., Riley, W. J., Sacks, W. J., Shi, M., Vertenstein, M., Wieder, W. R., Xu, C., Ali, A. A., Badger, A. M., Bisht, G., van den Broeke, M., Brunke, M. A., Burns, S. P., Buzan, J., Clark, M., Craig, A., Dahlin, K., Drewniak, B., Fisher, J. B., Flanner, M., Fox, A. M., Gentine, P., Hoffman, F., Keppel-Aleks, G., Knox, R., Kumar, S., Lenaerts, J., Leung, L. R., Lipscomb, W. H., Lu, Y., Pandey, A., Pelletier, J. D., Perket, J., Randerson, J. T., Ricciuto, D. M., Sanderson, B. M., Slater, A., Subin, Z. M., Tang, J., Thomas, R. Q., Val Martin, M., and Zeng, X.: The Community Land Model Version 5: Description of New Features, Benchmarking, and Impact of Forcing Uncertainty, Journal of Advances in Modeling Earth Systems, 11, 4245–4287, https://doi.org/10.1029/2018MS001583, 2019.

Lee, H., Swenson, S. C., Slater, A. G., and Lawrence, D. M.: Effects of excess ground ice on projections of permafrost in a warming climate, Environmental Research Letters, 9, 124006, 10.1088/1748-9326/9/12/124006, 2014.

Lin, Z., Gao, Z., Fan, X., Niu, F., Luo, J., Yin, G., and Liu, M.: Factors controlling near surface ground-ice characteristics in a region of warm permafrost, Beiluhe Basin, Qinghai-Tibet Plateau, Geoderma, 376, 114540, https://doi.org/10.1016/j.geoderma.2020.114540, 2020.

Lin, Z., Gao, Z., Niu, F., Luo, J., Yin, G., Liu, M., and Fan, X.: High spatial density ground thermal measurements in a warming permafrost region, Beiluhe Basin, Qinghai-Tibet Plateau, Geomorphology, 340, 1–14, https://doi.org/10.1016/j.geomorph.2019.04.032, 2019.

Luo, J., Niu, F., Lin, Z., Liu, M., Yin, G., and Gao, Z.: Abrupt increase in thermokarst lakes on the central Tibetan Plateau over the last 50 years, CATENA, 217, 106497, https://doi.org/10.1016/j.catena.2022.106497, 2022.

Morgenstern, N. R. and Nixon, J. F.: One-dimensional Consolidation of Thawing Soils, Canadian Geotechnical Journal, 8, 558–565, 10.1139/t71-057, 1971.

Nelson, F. E., Anisimov, O. A., and Shiklomanov, N. I.: Subsidence risk from thawing permafrost, Nature, 410, 889–890, 10.1038/35073746, 2001.

Nitzbon, J., Westermann, S., Langer, M., Martin, L. C. P., Strauss, J., Laboor, S., and Boike, J.: Fast response of cold ice-rich permafrost in northeast Siberia to a warming climate, Nature Communications, 11, 2201, 10.1038/s41467-020-15725-8, 2020.

Niu, F., Lin, Z., Liu, H., and Lu, J.: Characteristics of thermokarst lakes and their influence on permafrost in Qinghai–Tibet Plateau, Geomorphology, 132, 222–233, https://doi.org/10.1016/j.geomorph.2011.05.011, 2011.

O'Neill, H. B., Smith, S. L., Burn, C. R., Duchesne, C., and Zhang, Y.: Widespread Permafrost Degradation and Thaw Subsidence in Northwest Canada, Journal of Geophysical Research: Earth Surface, 128, e2023JF007262, https://doi.org/10.1029/2023JF007262, 2023.

Obu, J., Westermann, S., Bartsch, A., Berdnikov, N., Christiansen, H. H., Dashtseren, A., Delaloye, R., Elberling, B., Etzelmüller, B., Kholodov, A., Khomutov, A., Kääb, A., Leibman, M. O., Lewkowicz, A. G., Panda, S. K., Romanovsky, V., Way, R. G., Westergaard-Nielsen, A., Wu, T., Yamkhin, J., and Zou, D.: Northern Hemisphere permafrost map based on TTOP modelling for 2000–2016 at 1 km2 scale, Earth-Science Reviews, 193, 299–316, https://doi.org/10.1016/j.earscirev.2019.04.023, 2019.

Painter, S. L., Coon, E. T., Khattak, A. J., and Jastrow, J. D.: Drying of tundra landscapes will limit subsidence-induced acceleration of permafrost thaw, Proceedings of the National Academy of Sciences, 120, e2212171120, 10.1073/pnas.2212171120, 2023.

Painter, S. L., Coon, E. T., Atchley, A. L., Berndt, M., Garimella, R., Moulton, J. D., Svyatskiy, D., and Wilson, C. J.:

https://doi.org/10.5194/egusphere-2026-3345
Preprint. Discussion started: 15 September 2026


Integrated surface/subsurface permafrost thermal hydrology: Model formulation and proof-of-concept simulations, Water Resources Research, 52, 6062–6077, https://doi.org/10.1002/2015WR018427, 2016.

Schuur, E. A. G., McGuire, A. D., Schädel, C., Grosse, G., Harden, J. W., Hayes, D. J., Hugelius, G., Koven, C. D., Kuhry, P., Lawrence, D. M., Natali, S. M., Olefeldt, D., Romanovsky, V. E., Schaefer, K., Turetsky, M. R., Treat, C. C., and Vonk, J. E.: Climate change and the permafrost carbon feedback, Nature, 520, 171–179, 10.1038/nature14338, 2015.

Smith, S. L., O'Neill, H. B., Isaksen, K., Noetzli, J., and Romanovsky, V. E.: The changing thermal state of permafrost, Nature Reviews Earth & Environment, 3, 10–23, 10.1038/s43017-021-00240-1, 2022.

Streletskiy, D. A., Maslakov, A., Grosse, G., Shiklomanov, N. I., Farquharson, L., Zwieback, S., Iwahana, G., Bartsch, A., Liu, L., Strozzi, T., Lee, H., and Debolskiy, M. V.: Thawing permafrost is subsiding in the Northern Hemisphere—review and perspectives, Environmental Research Letters, 20, 013006, 10.1088/1748-9326/ada2ff, 2025.

Sun, Z., Zhao, L., Hu, G., Zhou, H., Liu, S., Qiao, Y., Du, E., Zou, D., and Xie, C.: Numerical Simulation of Thaw Settlement and Permafrost Changes at Three Sites Along the Qinghai-Tibet Engineering Corridor in a Warming Climate, Geophysical Research Letters, 49, e2021GL097334, https://doi.org/10.1029/2021GL097334, 2022.

Teng, Y. C., Teng, Z. C., Liu, Y., Liu, X. Y., Zhou, Y. D., Liu, J. L., and Li, B.: A Review of the Research on Thermo-Hydro-Mechanical Coupling for the Frozen Soil, Geofluids, 2022, 8274137, https://doi.org/10.1155/2022/8274137, 2022.

Tubini, N. and Gruber, S.: Simulating soil heat transfer with excess ice, erosion and deposition, guaranteed energy conservation, adaptive mesh refinement, and accurate spin-up (FreeThawXice1D), EGUsphere, 2025, 1–31, 10.5194/egusphere-2025-2649, 2025.

Turetsky, M. R., Abbott, B. W., Jones, M. C., Anthony, K. W., Olefeldt, D., Schuur, E. A. G., Grosse, G., Kuhry, P., Hugelius, G., Koven, C., Lawrence, D. M., Gibson, C., Sannel, A. B. K., and McGuire, A. D.: Carbon release through abrupt permafrost thaw, Nature Geoscience, 13, 138–143, 10.1038/s41561-019-0526-0, 2020.

Walvoord, M. A. and Kurylyk, B. L.: Hydrologic Impacts of Thawing Permafrost—A Review, Vadose Zone Journal, 15, vzj2016.2001.0010, https://doi.org/10.2136/vzj2016.01.0010, 2016.

Westermann, S., Langer, M., Boike, J., Heikenfeld, M., Peter, M., Etzelmüller, B., and Krinner, G.: Simulating the thermal regime and thaw processes of ice-rich permafrost ground with the land-surface model CryoGrid 3, Geosci. Model Dev., 9, 523–546, 10.5194/gmd-9-523-2016, 2016.

Westermann, S., Ingeman-Nielsen, T., Scheer, J., Aalstad, K., Aga, J., Chaudhary, N., Etzelmüller, B., Filhol, S., Kääb, A., Renette, C., Schmidt, L. S., Schuler, T. V., Zweigel, R. B., Martin, L., Morard, S., Ben-Asher, M., Angelopoulos, M., Boike, J., Groenke, B., Miesner, F., Nitzbon, J., Overduin, P., Stuenzi, S. M., and Langer, M.: The CryoGrid community model (version 1.0) – a multi-physics toolbox for climate-driven simulations in the terrestrial cryosphere, Geosci. Model Dev., 16, 2607–2647, 10.5194/gmd-16-2607-2023, 2023.

Yin, G.-A., Niu, F.-J., Lin, Z.-J., Luo, J., and Liu, M.-H.: Data-driven spatiotemporal projections of shallow permafrost based on CMIP6 across the Qinghai–Tibet Plateau at 1 km2 scale, Advances in Climate Change Research, 12, 814–827, 2021a.

Yin, G., Niu, F., Lin, Z., Luo, J., and Liu, M.: Effects of local factors and climate on permafrost conditions and distribution in Beiluhe basin, Qinghai-Tibet Plateau, China, Science of The Total Environment, 581-582, 472–485, https://doi.org/10.1016/j.scitotenv.2016.12.155, 2017.

Yin, G., Niu, F., Luo, J., Wang, J., Liu, M., Dong, T., Cao, Y., and Li, A.: High potential for pile-bearing capacity loss and ground subsidence over permafrost regions across the Northern Hemisphere, Global and Planetary Change, 226, 104156, https://doi.org/10.1016/j.gloplacha.2023.104156, 2023.

Yin, G., Ju, X., Niu, F., Lin, Z., Luo, J., Gao, Z., Yan, H., Wang, Y., and Ni, W.: Widespread weakening of soil-atmosphere thermal coupling and its response to climate warming on the Qinghai-Tibetan plateau, Agricultural and Forest Meteorology, 376, 110925, https://doi.org/10.1016/j.agrformet.2025.110925, 2026.

Yin, G. ThawCoupler-1D (v1.0): A physically-based one-dimensional coupled thermo-mechanical model for simulating thaw subsidence in permafrost, Zenodo [code], https://doi.org/10.5281/zenodo.20622154, (2026).

Yu, F., Guo, P., Lai, Y., and Stolle, D.: Frost heave and thaw consolidation modelling. Part 1: A water flux function for frost heaving, Canadian Geotechnical Journal, 57, 1581–1594, https://doi.org/10.1139/cgj-2019-0218, 2019.

Yu, F., Guo, P., Lai, Y., and Stolle, D.: Frost heave and thaw consolidation modelling. Part 2: One-dimensional thermohydromechanical (THM) framework, Canadian Geotechnical Journal, 57, 1595–1610, 10.1139/cgj-2019-0306,

https://doi.org/10.5194/egusphere-2026-3345
Preprint. Discussion started: 15 September 2026


2020.

Zhao, Y., Nan, Z., Ji, H., Chen, Y., Ou, M., and Li, D.: A Hybrid Modeling Approach for Improved Simulation of Thermal-Hydrological Dynamics in Active Layer on the Qinghai-Tibet Plateau, Water Resources Research, 61, e2025WR040288, https://doi.org/10.1029/2025WR040288, 2025.

Zhao, Y., Zheng, C., Gelfan, A., Watanabe, K., Liu, H., Wright, S., Wu, X., Quinton, W., Wang, Y., Yi, S., Zhang, Y., Shi, Y., and Jiao, W.: Frozen Soil Hydrological Processes and Their Effects: A Review and Synthesis, Reviews of Geophysics, 64, e2024RG000839, https://doi.org/10.1029/2024RG000839, 2026.